
On the influence of robustness measures on shape optimization with stochastic uncertainties

C. Schillings*¹ and V. Schulz**¹

¹ Universität Trier, Universitätsring 15, 54296 Trier, Germany.

The unavoidable presence of uncertainties poses several difficulties to the numerical treatment of optimization tasks. In this paper, we discuss a general framework attacking the additional computational complexity of the treatment of uncertainties within optimization problems considering the specific application of optimal aerodynamic design. Appropriate measure of robustness and a proper treatment of constraints to reformulate the underlying deterministic problem are investigated. In order to solve the resulting robust optimization problems, we propose an efficient methodology based on a combination of adaptive uncertainty quantification methods and optimization techniques, in particular generalized one-shot ideas. Numerical results investigating the reliability and efficiency of the proposed method as well as the influence of different robustness measures on the resulting optimized shape will be presented.

1 Introduction

Recently, aerodynamic shape optimization is a very active research field facing the challenges from highly demanding computational fluid dynamics problems, from optimization with partial differential equations as constraints as well as from the proper treatment of uncertainties. Due to increasing computing power and advancing algorithms, the numerical flow simulation has reached a highly sophisticated level and is therefore established as an indispensable tool for the development of new and for the improvement of existing airplanes. Further, the introduction of gradient computation via adjoint approach allows to efficiently evaluate derivatives needed in gradient-based optimization (cf. [17, 21, 22, 56, 59]). Besides standard optimization routines, which on average require 20-40 flow simulations, fast optimization methods based on one-shot ideas are available, too (see e.g. [20, 24, 66, 72]). They have the potential to reduce the overall costs of the optimization to just a few flow simulations. The one-shot method is based on approximate reduced SQP iterations solving the necessary optimality conditions simultaneously. However, a deterministic approach ignores the fact that there are stochastic and unknown variations in the problem. The conditions of operation are not known exactly, i.e. variations of the macroscopic flight conditions like the Mach number or the angle of attack may occur. The geometry itself undergoes unknown operational changes due to wear and tear and manufacturing inaccuracies. All these deviations from assumed setpoints of the deterministic optimization may render the supposedly optimal solution worthless, since their conclusions are not realized in practice. The proper treatment of these uncertainties within a numerical context is a very important challenge.

* claudia.schillings@uni-trier.de, Phone: +49 651 201 3440, Fax: +49 651 201 3966

** volker.schulz@uni-trier.de, Phone: +49 651 201 3484, Fax: +49 651 201 3966

In this paper, we propose a general framework for the proper treatment of uncertainties within a numerical context for the specific application of optimal aerodynamic design. The approach is based on an efficient combination of uncertainty quantification and highly sophisticated optimization techniques. Building on previous work, see [62, 63, 67], a methodology will be discussed enabling robust design for a broad class of robust formulations.

In recent times, robust optimization has become a very active area of research, where concepts of robustness have been developed independently in different scientific disciplines, see e.g. [4, 5, 6, 7, 12, 57, 60, 61, 71] and the references therein. In the aerodynamic context, uncertainty quantification methods have attracted a lot of attention so far and are the subject of numerous studies (cf. [38, 44, 46, 48, 51, 52, 76]), whereas robust aerodynamic design, in particular with respect to uncertain variations of the shape itself, is considered only in a few papers, see [25, 31, 40, 41, 44, 46, 55, 77].

In this paper, we will give insight into significant enhancements of robust gradient-based shape optimization methods providing a general framework in order to identify and quantify uncertainties arising in optimal aerodynamic design tasks, as well as to formulate appropriate robust counterparts of the deterministic problem and to efficiently solve the resulting optimization problems.

The paper is organized as follows: The first part is devoted to the identification of uncertainties and proper treatment within optimization tasks. Appropriate mathematical models of the uncertainties as well as robust formulations of the shape optimization problem will be discussed. Subsequently, we will introduce the ingredients of the optimization methodology, where the focus is on the adaption, enhancements and efficient combination of uncertainty quantification and optimization techniques. Finally, numerical results demonstrating the reliability and efficiency of the proposed method in a 2D industrial test case are presented. Further, we will investigate the influence of different measure of robustness on the resulting optimized shape providing an important contribution to achieve the desired grade of robustness in design tasks.

2 Deterministic aerodynamic shape optimization problem

The deterministic aerodynamic shape optimization problem of the following discrete form

$$\min_{y,p} f(y,p) \tag{1}$$

$$\text{s.t. } c(y,p) = 0 \tag{2}$$

$$h(y,p) \geq 0. \tag{3}$$

is considered. The variable $y \in \mathbb{R}^{n_y}$ denotes the discrete state variable in conservative form, which means they indicate the conservative quantities in each grid point. The design variables $p \in \mathbb{R}^{n_p}$ describe the shape to be optimized. As parametrization of the shape, an analytical approach introduced by Hicks and Henne [30] based on parametrizing the geometry using the weighted sum of a set of smooth (analytical) functions is used. Then, the design variables are the multipliers of the various Hicks-Henne functions deforming the camberline of the profile. The proposed methodology for robust optimization as well as the modeling of the uncertainty sources do not rely on the specific parametrization used. Thus, more sophisticated parametrizations, e.g. a direct approach (cf. [64, 65]), also fit in this framework. We think

of equation (2) as the flow equation, more precisely $c : \mathbb{R}^{n_y} \times \mathbb{R}^{n_p} \rightarrow \mathbb{R}^{n_y}$, represents the Euler or Navier-Stokes equation with appropriate boundary conditions. The objective in (1) $f : \mathbb{R}^{n_y} \times \mathbb{R}^{n_p} \rightarrow \mathbb{R}$ is the drag coefficient to be minimized and the inequality constraint (3) represents the lift requirements, that means $h : \mathbb{R}^{n_y} \times \mathbb{R}^{n_p} \rightarrow \mathbb{R}$ denotes the lift coefficient minus a target lift coefficient.

The state of the art in aerodynamic design is defined by deterministic gradient based design optimization, where the gradient information is produced by an adjoint approach

$$\frac{df}{dp}(y(p), p) = \frac{\partial f}{\partial p} - \lambda^\top \frac{\partial c}{\partial p},$$

where λ solves the adjoint equation $\left(\frac{\partial c}{\partial y}\right)^\top \lambda - \left(\frac{\partial f}{\partial y}\right)^\top = 0$. Details on adjoints in aerodynamic shape optimization can be found e.g. in [17, 21, 32, 33, 56]. The arising optimization problems (1 - 3) are solved using an one-shot approach, which is based on partially reduced SQP iterations (cf. [20, 24, 66, 72]). In [20], it is shown that the overall numerical effort of the optimization using the one-shot method can be reduced to 4-5 exact solutions of the flow equations (simulations) compared to black-box methods, which require over 30 simulations. We will generalize the one-shot approach to the robust aerodynamic optimization problems (see section 6) allowing the use of a very efficient optimization method in the robust framework.

3 Uncertainties in aerodynamic design

In order to formulate the robust design optimization problem, the boundary conditions and input parameters are analyzed to identify the uncertainties, which cannot be avoided at all before constructing an aircraft. We will focus on shape optimization problems influenced by aleatory uncertainties, which arise due to natural, unpredictable variations of the boundary conditions. Definitions and classification of errors and uncertainties in the aerodynamic framework can be found e.g. in [2, 54]. Additional knowledge cannot reduce aleatory uncertainties, but it may be useful in getting a better characterization of the variability. Further, we distinguish between uncertainties with respect to the flight conditions and geometrical uncertainties. The main characteristics of the macroscopic flight conditions are angle of incidence, the velocity (Mach number) of the plane, the density and the Reynolds number. The uncertainty of these parameters mostly results from atmospheric turbulences, which can occur during a flight. On the other hand, we consider the shape itself as an uncertainty source. The real shape may vary from the planned shape due to manufacturing tolerances, temporary factors like icing or fatigue of material. Since there are so many factors having effects on the shape, this uncertainty has to be considered in the optimization problem in order to produce a design, which is robust to small perturbations of the shape itself. In literature, there can be found only a few papers on this topic investigating the influence of variations of the profile (cf. [26, 46]). The treatment of these uncertainties within the optimization framework requires a mathematical description of the variations. In order to avoid a parametrization of the uncertainties, which would lead to a reduction of the space of realizations, a stochastic approach is chosen. Furthermore, this approach allows to adapt the model to new information of the uncertain parameter, e.g. if new measurements are available, so that a general framework of robust aerodynamic design can be developed.

3.1 Stochastic models of of the identified uncertainties

The uncertainties with respect to the flight conditions, the scalar-valued uncertainties, e.g. the Mach number, are modeled as real-valued, continuous random variables

$$s : \mathcal{O} \rightarrow \mathbb{R}, \quad (4)$$

defined on a given probability space $(\mathcal{O}, Y, \mathcal{P})$. They are characterized by a given probability density function

$$\varphi : \mathbb{R} \rightarrow \mathbb{R}. \quad (5)$$

We assume (mainly due to the lack of statistical data) a truncated normal distribution of the perturbations ensuring that the realizations lie in between the given bounds. Furthermore, the mean value of the random variable corresponds with the value of the deterministic model. These assumptions are widely used in order to describe uncertainties in CFD (cf. [46]). Nevertheless, the model needs to be adapted to measurements, if available.

The geometrical uncertainties are described by a transformed Gaussian random field of perturbations denoted by

$$s : \Gamma \times \mathcal{O} \rightarrow \mathbb{R},$$

where Γ denotes the shape of the profile and $(\mathcal{O}, Y, \mathcal{P})$ is a given probability space. The following assumption

$$s_l \leq s(x, \zeta) \leq s_u$$

is made guaranteeing the boundedness of the variations. Then, we consider a transformation of a Gaussian random field ψ of the form

$$s(x, \zeta) = \Theta(x, \psi(x, \zeta)) = F_{s(x)}^{-1}(\Phi(\psi(x, \zeta))), \quad (6)$$

such that $s(x, \zeta)$ has marginal distribution $F_{s(x)}$, where $F_{s(x)}$ ensures the boundedness of the perturbations and Φ denotes the Gaussian distribution function. The Gaussian random field ψ is determined by its mean $\mathbb{E}(\psi(x, \zeta)) = \psi_0(x)$ and covariance function $cov(x, y)$. Hence, a perturbed geometry is given by

$$v(x, \zeta) = x + s(x, \zeta) \cdot n(x), \quad \forall x \in \Gamma, \zeta \in \mathcal{O} \quad (7)$$

with $n(x)$ normal vector in x . Transformation of random fields ensuring boundedness of the realizations is a common techniques in literature, see e.g. [49, 3] and the references therein for more details. In the numerical results, an example of the model (6) in a 2D test case will be provided, where more details will be given on the chosen distribution function $F_{s(x)}$. The methodology suggested in this paper does not rely on a specific choice of the nonlinear transformation, so that arbitrary transformations can be used to describe the perturbations of the shape.

4 Robust formulation of the aerodynamic shape optimization problem

There is a variety of ways how optimization problems under uncertainties can be formulated. We will discuss several robust formulations of the general aerodynamic design optimization problem (1 - 3) based on probabilistic models of the uncertainties introduced in section 3.

In a first naive approach, we consider the general deterministic problem formulation (1 - 3) influenced by stochastic perturbations. For the sake of simplicity, the discussion below is restricted to random variables. The generalization of the formulations to random vectors and random fields is straightforward. We assume that the dependence of the uncertain parameter can arise in all aspects, i.e. a naive stochastic variant might be rewritten as

$$\min_{y,p} f(y, p, s(\zeta)) \quad (8)$$

$$\text{s.t. } c(y, p, s(\zeta)) = 0 \quad (9)$$

$$h(y, p, s(\zeta)) \geq 0, \quad (10)$$

where $s : \mathcal{O} \rightarrow \mathbb{R}$ is a real-valued, continuous random variable defined on a given probability space (\mathcal{O}, Y, P) and characterized by a given probability density function $\varphi : \mathbb{R} \rightarrow \mathbb{R}$. This formulation still treats the uncertain parameter as an additional fixed parameter. As the flow solution and consequently the lift and drag are dependent of the random input variable, these quantities itself become random vectors and random variables, respectively. Further, the state vector y also depends on the uncertain quantity s , so that there is a different y_s for each realization of the random variable s :

$$\min_{y(s(\zeta)),p} f(y(s(\zeta)), p, s(\zeta)) \quad (11)$$

$$\text{s.t. } c(y(s(\zeta)), p, s(\zeta)) = 0 \quad (12)$$

$$h(y(s(\zeta)), p, s(\zeta)) \geq 0. \quad (13)$$

The goal of robust optimization is now to find an optimal solution of problem (8 - 10), which is stable with respect to stochastic variations in s . Hence, the main task is to define an appropriate measure of robustness and proper treatment of constraints to reformulate problem (8 - 10)

$$\min_{y(s(\zeta)),p} \mathcal{R}(f(y(s(\zeta)), p, s(\zeta))) \quad (14)$$

$$\text{s.t. } c(y(s(\zeta)), p, s(\zeta)) = 0 \quad (15)$$

$$H(y(s(\zeta)), p, s(\zeta)) \geq 0. \quad (16)$$

and make it mathematically tractable. In literature, there can be found various definitions of robustness, see e.g. [4, 6, 7, 60, 61] and the references therein for more details. The most common measures of robustness \mathcal{R} are the following ones:

- Worst-case risk measure:

$$\min_{y(s(\zeta)),p} \max_{s(\zeta)} (f(y(s(\zeta)), p, s(\zeta))) \quad (17)$$

- Expectation measure:

$$\min_{y(s(\zeta)), p} \mathbb{E}(f(y(s(\zeta)), p, s(\zeta))) \quad (18)$$

- Mean-risk approach:

i.e.

- Mean-variance :

$$\min_{y(s(\zeta)), p} \mathbb{E}(f(y(s(\zeta)), p, s(\zeta))) + c\mathbb{V}(f(y(s(\zeta)), p, s(\zeta))) \quad (19)$$

- Expected excess:

$$\min_{y(s(\zeta)), p} \mathbb{E}(\max\{f(y(s(\zeta)), p, s(\zeta)) - \eta, 0\}) \quad (20)$$

The worst-case risk measure may lead to overly conservative designs, so that we will focus here on the expectation measure and mean-risk approach and provide a general methodology to handle these measures of robustness.

There are also several possibilities for a proper treatment of constraints in a robust context (cf. e.g. [4, 57, 29]):

- Expectation constraints:

$$h(y, p, \mathbb{E}(s(\zeta))) \geq 0 \quad (21)$$

- Worst-case constraints:

$$h(y, p, s(\zeta)) \geq 0, \quad \forall \zeta \quad (22)$$

- Robust optimization:

$$h(y, p, s(\zeta)) \geq 0, \quad \forall \zeta \in H \quad (23)$$

for a given set H .

- Chance-constraints:

$$\mathbb{P}(h(y, p, s(\zeta)) \geq 0) \geq P_0 \quad (24)$$

with a prescribed probability P_0 .

Since the mean value of the random input corresponds to the nominal point of the deterministic model, the expectation constraint (21) coincides with the lift requirement of the deterministic shape optimization problem (cp. (3)). In contrast to the worst-case and robust optimization constraints considering the feasibility for all realizations (in a given set H) in the sense of almost everywhere, chance constraints leave some flexibility with respect to the inequality restrictions, which are only required to hold with a certain probability P_0 . So far, chance constraints are used mainly for weakly nonlinear optimization problems (cf. [29, 34]) and

are addressed only in a few papers in the context of aerodynamic shape optimization due to the numerical difficulties arising from the check for feasibility for a given design vector as well as from the structure of the feasible set defined by the chance constraint, see [1, 58, 67, 62] for more details. Hence, we will focus in this paper on the development of methods to handle robust optimization and worst-case constraints. The resulting robust aerodynamic shape optimization problem reads

$$\min_{y(s(\zeta)), p} \mathcal{R}(f(y(s(\zeta)), p, s(\zeta))) \quad (25)$$

$$\text{s.t.} \quad c(y(s(\zeta)), p, s(\zeta)) = 0 \quad (26)$$

$$h(y(s(\zeta)), p, s(\zeta)) \geq 0 \quad \forall \zeta \in H, \quad (27)$$

where the robustness measure \mathcal{R} is given by (18), (19) or (20). We can state the following observations:

- The evaluation of the measure of robustness in the objective function requires the computation of statistics, i.e. high-dimensional integrals, which cannot be solved analytically.
- In order to ensure the feasibility over the whole range of variations of the uncertain quantity s , the influence of the uncertain parameter has to be quantized to solve the lower level optimization problem arising in the robust optimization problem (25 - 27).
- Considering geometrical uncertainties modeled as a random field of perturbations, a representation of the spatially distributed uncertainties in a finite number of random variables is required for a numerical treatment.

For these tasks, uncertainty quantification methods are discussed in the next section.

5 Uncertainty quantification methods

The purpose of uncertainty quantification methods is the determination of the effect of uncertainties in the input data on quantities of interest in the output of a simulation. In the following, a general framework in order to handle the robust optimization problem (25 - 27) will be discussed. Uncertainty quantification in CFD computations is a fast growing field of research in the last years, since classical methods are often inadequate for application to CFD problems due to their high amount of computational effort. The proposed methods in literature can be classified into two classes: the first one directly applies statistical methods to the simulation (e.g. Monte Carlo methods, response surface methods,...), whereas the second one solves the stochastic equation (e.g. polynomial chaos, stochastic operator expansion,...). We will concentrate in this paper on a combination of both classes leading to an efficient treatment of the robust aerodynamic shape optimization problem. First, we will discuss a goal-oriented variant of the Karhunen-Loève expansion, which is the most effective approach concerning the convergence rate (in the case of linear approximations, see e.g. [19]). The Karhunen-Loève expansion is based on a spectral decomposition of the covariance kernel, hence the covariance function of the output has to be known which is not the case in most of the applications. Due to this fact, the Karhunen-Loève expansion is not a suitable choice in order to compute the statistics of the solution in our application. But this approach can be used to approximate

the input random field describing the geometrical uncertainties in a finite number of random variables.

Polynomial chaos and stochastic collocation techniques are the most used methods to propagate uncertainties in numerical simulations due to their computational efficiency and strong mathematical basis. We will give a brief overview of these methods and refer to standard textbooks for an exhaustive introduction to this topic, see e.g. [19]. Both methods represent the stochastic output in a finite series of polynomials in the stochastic variable

$$f(p, s(\zeta)) \approx \sum_{i=1}^{N_c} \tilde{f}(p) \mathbf{P}_i(s(\zeta))$$

where N_P denotes the truncation order of the expansion, \mathbf{P} are multivariate polynomials. The dependency of the objective function f on the state variables y is disregarded for simplicity reasons, assuming that the implicit function theorem can be applied. Polynomial chaos and stochastic collocation methods split the deterministic part \tilde{f} and the stochastic part \mathbf{P} and differ in the choice of the polynomial basis and the computation of the deterministic coefficients \tilde{f} . Stochastic collocation expansion is formed as a sum of multi-dimensional interpolation polynomials, where the coefficients are determined by a collocation method. The polynomial chaos method uses polynomials, which are orthogonal with respect to the probability density function of the uncertain parameters. Stochastic Collocation and (non-intrusive) polynomial chaos allow to use the flow solver as a black box, which is an important feature concerning our application. Numerically comparing these two approaches in a 2D test case, we observed a similar approximation quality of both methods (consistent with results published, e.g. in [13, 45]). However, the stochastic collocation approach suffers from two main shortcomings, the dependence of the interpolation terms with the number of collocation points and the strong influence of the choice of interpolation points on the convergence properties, so that the polynomial chaos seems to be of advantage in our application and we will concentrate on this uncertainty quantification method in the following. The last part of this section is devoted to discretization techniques of the probability space in order to approximate high dimensional integrals arising from the computation of statistics as well as from the determination of the polynomial chaos presentation. The focus will be on adaptive sparse grids and Monte Carlo techniques.

5.1 Goal-oriented Karhunen-Loève expansion

The Karhunen-Loève expansion, also known as Proper Orthogonal Decomposition, represents the random field as a infinite linear combination of orthogonal functions chosen as the eigenfunctions of the covariance function. The approach introduced by [35] and [42, 43] is a very common technique in the context of uncertainty quantification and discussed in many text books, see e.g. [19]. The expansion of the random field ψ is given by

$$\psi(x, \zeta) = \psi_0(x) + \sum_{i=1}^{\infty} \sqrt{\lambda_i^{KL} z_i^{KL}}(x) X_i(\zeta), \quad (28)$$

where $\lambda_1^{KL} \geq \lambda_2^{KL} \geq \dots \geq \lambda_i^{KL} \geq \dots \geq 0$ and z_i^{KL} are the eigenvalues and eigenfunctions of the covariance function cov , i.e.

$$\int_{\Gamma} cov(x, y) z_i^{KL}(y) = \lambda_i^{KL} z_i^{KL}(x), \quad (29)$$

X_i are uncorrelated random variables

$$X_i(\zeta) = \frac{1}{\sqrt{\lambda_i^{KL}}} \int_{\Gamma} (\psi(x, \zeta) - \psi_0(x)) z_i^{KL}(x) dx, \quad j = 1, 2, \dots \quad (30)$$

with zero mean and unit variance, and ψ_0 denotes the mean value of the random field. In the special case of a Gaussian random field, uncorrelated implies independent, which is an important property concerning the evaluation of high dimensional integrals. The truncated Karhunen-Loève expansion

$$\psi_d(x, \zeta) = \psi_0(x) + \sum_{i=1}^{N_{KL}} \sqrt{\lambda_i^{KL}} z_i^{KL}(x) X_i(\zeta), \quad (31)$$

converges to ψ in variance uniformly in x , i.e. in $L^\infty(\Gamma) \times L^2(\mathcal{O})$

$$\lim_{d \rightarrow \infty} \left\{ \sup_{\Gamma} \int_{\mathcal{O}} (\psi - \psi_d)^2 d\mathcal{P}(\zeta) \right\} = \lim_{d \rightarrow \infty} \left\{ \sup_{\Gamma} \left(\sum_{j=d+1}^{\infty} \lambda_j^{KL} (z_j^{KL})^2 \right) \right\} = 0. \quad (32)$$

So, ψ_d may provide a suitable approximation of ψ , if the eigenvalues decay sufficiently fast, where estimates on the decay with respect to cov can be found in e.g. [68].

To further reduce the number of basis functions in the representation (31), which corresponds to the dimension of the underlying probability space, the influence on the quantity of interest in the output, the drag or lift coefficient, will be investigated, so that the orthogonal basis functions $\{z_i^{KL}\}$ can be chosen goal-oriented. Thus, the idea is to develop an error indicator for the individual eigenvectors reflecting the impact on the target value, following closely [62, 50]. The error analysis of the Karhunen-Loève expansion in (32) only gives the approximation error of the random field ψ , but not of the function of interest, e.g. f . We propose to use sensitivity information to capture the local behavior of the drag and lift, respectively, with respect to the eigenvectors

$$\eta_i := \frac{df}{dz_i^{KL}} = -\lambda^\top \frac{\partial c}{\partial z_i^{KL}} + \frac{\partial f}{\partial z_i^{KL}}, \quad \forall i = 1, \dots, d, \quad (33)$$

and

$$\eta_i := \frac{dh}{dz_i^{KL}} = -\lambda^\top \frac{\partial c}{\partial z_i^{KL}} + \frac{\partial h}{\partial z_i^{KL}}, \quad \forall i = 1, \dots, d, \quad (34)$$

respectively, where λ solves the adjoint equation. The adjoint equation is independent of i , hence it has to be solved only once and the indicator η_i is numerically cheap to evaluate. Now, the reduced basis \hat{z}^{KL} can be automatically selected, the eigenvector z_i^{KL} with a large value η_i has to be kept in the reduced basis, whereas a small value indicates that the basis vector can be rejected from the basis.

5.2 Non-intrusive polynomial chaos

Polynomial chaos expands the solution nonlinearly depending on the random vector s in a series of orthogonal polynomials with respect to the distribution of the random input vector s

$$f(p, s(\zeta)) = \sum_{i=1}^{\infty} \tilde{f}_i(p) \cdot \Phi_i(s(\zeta)) \quad (35)$$

with Φ_i orthogonal polynomials, $\tilde{f}_i(p)$ deterministic coefficient functions. Again, the dependency of the objective function f on the state variables y is disregarded for simplicity reasons. As equation (35) indicates, the method allows a separation of the deterministic and stochastic part of the solution. In practice, one truncates the infinite expansion at a finite number of random variables and computes the statistics approximately by

$$f_{PC}(p, s(\zeta)) = \sum_{i=1}^{N_{PC}} \tilde{f}_i(p) \cdot \Phi_i(s(\zeta)) . \quad (36)$$

The theory of polynomial chaos was first developed for the analysis of stochastic functions depending on Gaussian random variables (see [75]) and later generalized to arbitrary distribution functions (cf. e.g. [76, 73]). The convergence of the polynomial chaos expansion based on Hermite polynomials is ensured by the theorem of Cameron and Martin (see [11]). In the following, we will concentrate on the so called homogeneous polynomial chaos, as Gaussian random variables are used to describe the uncertainties in the application of interest and refer to literature concerning the generalized polynomial chaos theory. In order to determine the polynomial chaos representation (35) and (36), respectively, we compute the deterministic coefficient functions \tilde{f}_i in a non-intrusive way allowing to use the flow solver as black box. Based on the theorem of Cameron and Martin, the coefficient functions can be evaluated by numerically approximating the following integrals

$$\tilde{f}(p) = \frac{\langle f(p, \cdot), \Phi_k \rangle}{\langle \Phi_k^2 \rangle} \quad (37)$$

$$= \frac{1}{\langle \Phi_k^2 \rangle} \int_{\mathbb{R}^d} f(p, \nu) \Phi_k(\nu) \varphi_s(\nu) \, d\nu, \quad k = 1, \dots, N_{PC}. \quad (38)$$

In the following subsection, we will discuss an efficient method, adaptive sparse grids, to approximate high dimensional integrals like (38).

5.3 Discretization of the probability space

The determination of the deterministic polynomial chaos coefficients as well as statistics depending on the current design vector and the uncertain parameters are required in each iteration of the robust optimization. Since the arising multi-dimensional integrals cannot be solved analytically, we have to approximate them in an appropriate, efficient way. In literature, several possibilities in order to numerically compute the required integrals are proposed. The most common are: Monte Carlo simulation, respectively general Sampling methods, full tensor grid interpolation and sparse grid interpolation. Their efficiency depends on the dimension d of the probability space \mathcal{O} and on the properties of the integrand. As already shown

in previous publications (cf. [62, 63]), adaptive sparse grids provide an efficient approach in the application of interest and can be further improved by adaptive strategies. In the last part of this section, we will shortly introduce the well-known Monte Carlo method, which we will use to determine the expected excess (20) based on the polynomial chaos approximation.

5.3.1 Adaptive sparse grids

The idea of sparse grids is to combine quadrature formulas of high order in some dimensions with quadrature formulas of lower order in the other dimensions in such a way that the interpolation error is nearly the same as for full tensor products. Sparse grids were originally found by the Russian mathematician Smolyak [70] and extensively studied and further developed e.g. in [15, 10, 16, 18, 36]. The sparse integrand is given as:

$$\mathcal{S}(k, d)(f) = \sum_{k-d+1 \leq |\mathbf{i}| \leq k} (-1)^{k-|\mathbf{i}|} \cdot \binom{d-1}{k-|\mathbf{i}|} \cdot (\mathcal{Q}^{i_1} \otimes \dots \otimes \mathcal{Q}^{i_d})(f) \quad (39)$$

with $k \geq d$, $\mathbf{i} \in \mathbb{N}^d$ multi-index and $|\mathbf{i}| = \sum_{j=1}^d i_j$. The index i_j indicates the order in the j -th dimension, so the algorithm combines only those one-dimensional quadrature formulas, whose indices fulfill the constraint that the total sum across all dimensions is greater or equal $k-d+1$ and smaller or equal k . Using incremental interpolation formulas $\Delta^{\mathbf{i}}$, (39) can be transformed to

$$\mathcal{S}(k, d)(f) = \sum_{|\mathbf{i}| \leq k} (\Delta^{i_1} \otimes \dots \otimes \Delta^{i_d})(f) \quad (40)$$

$$= \mathcal{S}(k-1, d)(f) + \sum_{|\mathbf{i}|=k} (\Delta^{i_1} \otimes \dots \otimes \Delta^{i_d})(f) \quad (41)$$

with $\Delta^{\mathbf{i}} = \mathcal{Q}^{i+1} - \mathcal{Q}^{\mathbf{i}}$, $\mathcal{Q}^0 \equiv 0$ and $\mathcal{S}(d-1, d) \equiv 0$. The collection of all the interpolation points

$$\mathcal{H}(k, d) = \bigcup_{k-d+1 \leq |\mathbf{i}| \leq k} (G^{i_1} \times \dots \times G^{i_d}) \quad (42)$$

is called a sparse grid of level k , where $G^k = \{x_k | x_k \in \mathbb{R} \text{ interpolation point}\}$, $\#G^k = mk$. Using one-dimensional interpolatory quadrature formulas with positive weights as basis for the Smolyak algorithm, the approximation quality of the resulting sparse grid is of order

$$\epsilon(N) = O\left(N^{-k} \cdot (\log N)^{(k+1)(d-1)}\right) \quad (43)$$

with N number of sparse grid points, considering function classes \mathcal{W}_d^k with bounded mixed derivatives up to order k and $d > 1$ (cf. [74]). The sparse grid approach outperforms the conventional full tensor grids, which achieve an approximation quality of $O(N^{-\frac{k}{d}})$. Hence, the sparse grid approach overcomes the curse of dimensionality and is an appropriate choice for higher dimensional problems. Especially in combination with adaptive refinement strategies, which we will discuss in the following, the sparse grid method has the potential to reach a high approximation quality with less grid points than the other discussed sampling methods.

Dimension adaptive sparse grids The main advantage of the dimension adaptive refinement strategy is the fact that one can use problem dependent quadrature formulas in order to construct the adaptive sparse grid. In our application, the objective function, the drag, is multiplied by the Gaussian density function, so that Gaussian Hermite polynomials are optimal with respect to the weighting function.

First, a generalization of sparse grids will be introduced, which allows to weight the dimensions according to their importance on the target functional. The idea of generalized sparse grids and especially dimension adaptive sparse grid can be found in [10, 16, 18] and [36]. The original sparse grid of order k combines all the incremental functions, which sum up to order k , that means only those indices are considered, which are contained in the unit simplex $|\mathbf{i}| \leq k$. [14] and [18] suggest to allow a more general index set, which can be adaptively chosen with respect to the importance of each dimension.

An index set \mathbf{I} is called *admissible* if $\forall \mathbf{i} \in \mathbf{I}$

$$\mathbf{i} - e_j \in \mathbf{I}, \quad \forall 1 \leq j \leq d, i_j > 1,$$

where $e_j \in \mathbb{R}^d$ is the j -th unit vector. The generalized index set \mathbf{I} contains for an index \mathbf{i} all indices, which have smaller entries in one or more dimensions. Due to this fact, the incremental sparse grid formula (41) is still well defined for the new index sets and is given as

$$\mathcal{S}(k, d)(f) = \sum_{\mathbf{i} \in \mathbf{I}} (\Delta^{i_1} \otimes \cdots \otimes \Delta^{i_d})(f). \quad (44)$$

The generalized definition of sparse grids includes the original sparse grid and the full tensor grid definition. Then, the sparse grid is successively constructed, automatically computing an admissible index set in a dimension adaptive way, in the following way: Starting with the coarsest sparse grid, that means $\mathbf{I} = \{(0, \dots, 0)^\top\}$, and new indices are added step by step to the sparse grid, such that

- the new index set remains admissible
- the approximation error is reduced.

In the case of direct integration of statistics, we propose as adaptivity indicator to successively adapt the sparse grid based on the improvement of the quantity of interest

$$\mathcal{R}(f(y(s(\zeta)), p, s(\zeta))) = \int_{\mathcal{O}} r(f(y(s(\zeta)), p, s(\zeta))) d\mathcal{P}(\zeta)$$

, i.e. to measure the improvement by adding a new index to the sparse grid

$$\eta_{\mathbf{h}}^{SG} = \Delta_{\mathbf{i}}(r(f)) = (\Delta^{i_1} \otimes \cdots \otimes \Delta^{i_d})(r(f))$$

and stop, if $\|\eta_{\mathbf{h}}^{SG}\| < \epsilon$. In order to determine the deterministic coefficient functions of the polynomial chaos expansion, we propose to consider the following error indicator

$$\max\{\Delta_{\mathbf{i}}(\tilde{f}_0), \Delta_{\mathbf{i}}(\tilde{f}_1), \dots, \Delta_{\mathbf{i}}(\tilde{f}_{N^{PC}})\},$$

i.e. the sparse grid is successively adapted according to the largest error arising in the approximation of all polynomial chaos coefficients. The idea is to use the same sparse grid

for the determination of all coefficients, so that the information gained by an expensive flow simulation, which needs to be performed to improve the approximation quality for one specific coefficient function, can be used to improve the approximation quality for all coefficient functions.

Details on the algorithm can be found in [14, 62].

Locally refined sparse grids Below, we introduce a locally adaptive hierarchical sparse grid approach using piecewise multilinear hierarchical basis functions following closely [37, 47]. This method will be used to solve the lower level problem of (25 - 27) by a discretization approach. Linear hat functions are chosen as interpolation basis functions, which are transformed to a hierarchical basis, so that the sparse grid can be formulated in the following hierarchical form

$$\begin{aligned} \mathcal{S}(k, d)(f) &= \mathcal{S}(k-1, d)(f) + \sum_{|\mathbf{i}|=k} (\Delta^{i_1} \otimes \dots \otimes \Delta^{i_d})(f) \\ &= \mathcal{S}(k-1, d)(f) + \Delta\mathcal{S}(k, d)(f) \end{aligned}$$

with

$$\begin{aligned} \Delta\mathcal{S}(k, d)(f) &= \sum_{|\mathbf{i}|=k} \sum_{\mathbf{j} \in I_{hier}^{\mathbf{i}}} \underbrace{(a_{j_1}^{i_1} \otimes \dots \otimes a_{j_d}^{i_d})}_{a_{\mathbf{j}}^{\mathbf{i}}} \cdot \\ &\quad \cdot \underbrace{(f(Y_{j_1}^{i_1}, \dots, Y_{j_d}^{i_d}) - \mathcal{S}(k-1, d)(f)(Y_{j_1}^{i_1}, \dots, Y_{j_d}^{i_d}))}_{w_{\mathbf{j}}^{\mathbf{i}}}, \end{aligned} \quad (45)$$

where $I_{hier}^{\mathbf{i}} := \{\mathbf{j} \in \mathbb{N}^d : Y_{j_l}^{i_l} \in G_{\Delta}^{i_k} \text{ for } j_l = 1, \dots, m_{\Delta}^{i_l}, k = 1, \dots, d\}$, $G_{\Delta}^i = G^i \setminus G^{i-1}$, $m_{\Delta}^i = \#G_{\Delta}^i = m_i - m_{i-1}$, is a new set of multi-indices consistent with the multivariate hierarchical basis $\{a_{\mathbf{j}}^{\mathbf{i}} : \mathbf{j} \in I_{hier}^{\mathbf{i}}, \mathbf{o} \leq \mathbf{i}\}$ with $a_{\mathbf{j}}^{\mathbf{i}}$ one-dimensional linear hat functions. Similar to the dimension adaptive refinement algorithm, the sparse grid is successively constructed using the hierarchical surpluses $w_{\mathbf{j}}^{\mathbf{i}}$ as adaptivity indicator measuring the improvement gained by adding a new index to the grid. We refer to [37, 62] for more details.

5.3.2 Monte Carlo

Finally, we briefly discuss Monte Carlo methods for the sake of completeness, as we will use this method to approximate the expected excess (cf. 20) based on the representation of the objective function using the polynomial chaos expansion (36).

The expectation $\mathbb{E}(\max\{f_{PC}(p, s_d(\zeta)) - \eta, 0\})$ will be estimated by the mean over samples f_{PC}^i , $i = 1, \dots, M$ corresponding to M independent, normally distributed realizations of the random variables obtained by the Karhunen-Loève expansion. For practical convenience, the max-function is replaced by a smooth approximation

$$\widehat{\max}(f_{PC}(p, s_d(\zeta)) - \eta, 0) := \frac{1}{2}(\sqrt{(f_{PC}(p, s_d(\zeta)) - \eta)^2 + \epsilon} + f_{PC}(p, s_d(\zeta)) - \eta)$$

leading to

$$\mathbb{E}^{MC}(\widehat{\max}\{f_{PC}(p, s_d(\zeta)) - \eta, 0\}) = \frac{1}{M} \sum_{i=1}^M \widehat{\max}\{f_{PC}^i(p) - \eta, 0\}. \quad (46)$$

The convergence is ensured by the law of large numbers with the expected convergence rate $O(N^{-\frac{1}{2}})$, i.e. a quadrupling of the sample size halves the error. In general, Monte Carlo methods are not suitable in our application due to the large number of function evaluations required. Here, we propose to sample from the surrogate model resulting from the polynomial chaos expansion, so that (46) is very cheap to evaluate and therefore, the Monte Carlo method is an appropriate choice to determine (20). Detailed information on Monte Carlo as well as quasi Monte Carlo methods can be found e.g. in [23, 27, 53, 39].

6 Optimization method

Applying the uncertainty quantification methods discussed above, i.e. the polynomial chaos method in combination with dimension adaptive sparse grids to represent the objective function, locally refined sparse grids to construct a surrogate of the lift constraint and in the case of the expected excess as robustness measure, a Monte Carlo approach based on the polynomial chaos representation, we obtain the following discretized version of the robust optimization problem (25 - 27)

$$\min_{y_i, p} \sum_{i=1}^N f(y_i, p, s_i) \omega_i \quad (47)$$

$$\text{s.t.} \quad c(y_i, p, s_i) = 0, \quad \forall i \in \{0, \dots, N\} \quad (48)$$

$$h(y_0, p, s_0) \geq 0, \quad (49)$$

where s_0 approximates the solution of the lower level problem $\min_{s \in H} h(p, s)$ using a discretization approach based on locally refined sparse grids. In the robust optimization framework, the special structure of multiple-setpoint problems often arises as a result of the discretization of the probability space. A generalization of the one-shot approach to the multiple-setpoint problems exploiting the structure of the underlying problem will be introduced in this section. Numerical approaches to this problem class have already been proposed in [8, 9, 62, 67, 63]. For the sake of simplicity, we restrict the discussion to a problem of the form

$$\min_{y_1, y_2, p} \omega_1 \cdot f(y_1, p, s_1) + \omega_2 \cdot f(y_2, p, s_2) \quad (50)$$

$$\text{s.t.} \quad c(y_i, p, s_i) = 0, \quad i = 0, 1, 2 \quad (51)$$

$$h(y_0, p, s_0) \geq 0, \quad (52)$$

where s_i denotes the i -th setpoint. We can think of s_i as a realization of a random parameter, i.e. of the Mach number. The two setpoints in the objective function (50) are coupled via a weighted sum and the design variables p , which are the same for all set-points. In addition, the lift constraint is required at a third setpoint s_0 . The generalization to more setpoints is then obvious.

The corresponding Lagrangian of problem (50 - 52) is given by

$$\begin{aligned} \mathcal{L}(y_0, y_1, y_2, p, \lambda_0, \lambda_1, \lambda_2, \mu) = & \omega_1 \cdot f(y_1, p, s_1) + \omega_2 \cdot f(y_2, p, s_2) \\ & + \lambda_0^\top c(y_0, p, s_0) + \lambda_1^\top c(y_1, p, s_1) + \lambda_2^\top c(y_2, p, s_2) \\ & + \mu^\top h(y_0, p, s_0). \end{aligned}$$

Resulting from the necessary optimality conditions

$$\begin{aligned}\nabla_{y_i} \mathcal{L} &= 0, \quad i = 1, 2, 3 \\ \nabla_p \mathcal{L} &= 0 \\ c(y_i, p) = \nabla_{\lambda_i} \mathcal{L} &= 0, \quad i = 1, 2, 3 \\ h(y_0, p) = \nabla_{\mu} \mathcal{L} &= 0,\end{aligned}$$

we obtain the following KKT system

$$\begin{bmatrix} H_{y_0 y_0} & H_{y_0 y_1} & H_{y_0 y_2} & H_{y_0 p} & (C_{y_0}^0)^\top & 0 & 0 & (H_{y_0}^{lift})^\top \\ H_{y_1 y_0} & H_{y_1 y_1} & H_{y_1 y_2} & H_{y_1 p} & 0 & (C_{y_1}^1)^\top & 0 & 0 \\ H_{y_2 y_0} & H_{y_2 y_1} & H_{y_2 y_2} & H_{y_2 p} & 0 & 0 & (C_{y_2}^2)^\top & 0 \\ H_{p y_0} & H_{p y_1} & H_{p y_2} & H_{p p} & (C_p^0)^\top & (C_p^1)^\top & (C_p^2)^\top & (H_p^{lift})^\top \\ C_{y_0}^0 & 0 & 0 & C_p^0 & 0 & 0 & 0 & 0 \\ 0 & C_{y_1}^1 & 0 & C_p^1 & 0 & 0 & 0 & 0 \\ 0 & 0 & C_{y_2}^2 & C_p^2 & 0 & 0 & 0 & 0 \\ H_{y_0}^{lift} & 0 & 0 & H_p^{lift} & 0 & 0 & 0 & 0 \end{bmatrix} \begin{pmatrix} \Delta y_0 \\ \Delta y_1 \\ \Delta y_2 \\ \Delta p \\ \Delta \lambda_0 \\ \Delta \lambda_1 \\ \Delta \lambda_2 \\ \Delta \mu \end{pmatrix} = \begin{pmatrix} -\nabla_{y_0} \mathcal{L} \\ -\nabla_{y_1} \mathcal{L} \\ -\nabla_{y_2} \mathcal{L} \\ -\nabla_p \mathcal{L} \\ -c_0 \\ -c_1 \\ -c_2 \\ -h \end{pmatrix}, \quad (53)$$

where C^i denotes the Jacobian of the flow equation of the i -th setpoint. Approximating the Hessian of the Lagrangian in (53) by

$$\begin{bmatrix} H_{y_0 y_0} & H_{y_0 y_1} & H_{y_0 y_2} & H_{y_0 p} \\ H_{y_1 y_0} & H_{y_1 y_1} & H_{y_1 y_2} & H_{y_1 p} \\ H_{y_2 y_0} & H_{y_2 y_1} & H_{y_2 y_2} & H_{y_2 p} \\ H_{p y_0} & H_{p y_1} & H_{p y_2} & H_{p p} \end{bmatrix} \approx \begin{bmatrix} 0 & 0 & 0 & 0 \\ 0 & 0 & 0 & 0 \\ 0 & 0 & 0 & 0 \\ 0 & 0 & 0 & B \end{bmatrix},$$

and applying a block elimination, we obtain

$$\begin{aligned} & \begin{bmatrix} B & (H_p^{lift})^\top - (C_p^0)^\top (C_{y_0}^0)^{-\top} (H_{y_0}^{lift})^\top \\ ((H_p^{lift})^\top - (C_p^0)^\top (C_{y_0}^0)^{-\top} (H_{y_0}^{lift})^\top)^\top & 0 \end{bmatrix} \begin{pmatrix} \Delta p \\ \Delta \mu \end{pmatrix} \\ &= \begin{pmatrix} (C_p^0)^\top (C_{y_0}^0)^{-\top} \nabla_{y_0} \mathcal{L} + (C_p^1)^\top (C_{y_1}^1)^{-\top} \nabla_{y_1} \mathcal{L} + (C_p^2)^\top (C_{y_2}^2)^{-\top} \nabla_{y_2} \mathcal{L} - \nabla_p \mathcal{L} \\ -h - H_{y_0}^{lift} (C_{y_0}^0)^{-\top} c_0 \end{pmatrix}. \end{aligned}$$

Replacing $\Delta \mu$ by $\mu_{k+1} = \mu_k + \Delta \mu$ leads to

$$\begin{bmatrix} B & \gamma_h^{red} \\ (\gamma_h^{red})^\top & 0 \end{bmatrix} \begin{pmatrix} \Delta p \\ \mu_{k+1} \end{pmatrix} = \begin{pmatrix} -\gamma_f^{red} \\ -h - H_{y_0}^{lift} (C_{y_0}^0)^{-\top} c_0 \end{pmatrix},$$

with

$$\begin{aligned} \gamma_h^{red} &= (H_p^{lift})^\top - (C_p^0)^\top (C_{y_0}^0)^{-\top} (H_{y_0}^{lift})^\top \\ \gamma_f^{red} &= \omega_1 \cdot \gamma_{f^1}^{red} + \omega_2 \cdot \gamma_{f^2}^{red} \\ &= \omega_1 \cdot (\nabla_p f^1 - (C_p^1)^\top (C_{y_1}^1)^{-\top} \nabla_{y_1} f^1) + \omega_2 \cdot (\nabla_p f^2 - (C_p^2)^\top (C_{y_2}^2)^{-\top} \nabla_{y_2} f^2). \end{aligned}$$

We notice that the adjoint solution of

$$C_{y_i}^\top \sigma_{f^i} = -\nabla_{y_i} f^i, \quad i = 1, 2$$

and the lift coefficient

$$C_{y_0}^\top \sigma_h = -\nabla_{y_0} h$$

are to be solved independently, and then collected in the reduced gradients.

Therefore, the iterations in the adjoint solvers can be done in parallel for each setpoint s_i . Then, the update in the design variables is computed and distributed to all forward problems, which can again be performed in parallel. Hence, the amount of additional computational effort considering a multiple-setpoint optimization problem can be efficiently overcome by a parallelization of function evaluations and gradient computations of the different setpoints.

7 Summary of the methodology

All the ingredients we need to solve the robust aerodynamic shape optimization problem (25 - 27) were discussed in the previous sections. We will now give a short summary and overview of the whole methodology, which is based on a combination of uncertainty quantification methods and efficient optimization strategies:

1. The input random field modeling the uncertainties is approximated in a finite number of random variables using a goal-oriented Karhunen-Loève expansion.

$$s_d(x, \zeta) = \Theta \left(x, \psi_0(x) + \sum_{i=1}^d \sqrt{\hat{\lambda}_i^{KL}} \hat{z}_i^{KL}(x) X_i(\zeta) \right)$$

2. The drag with respect to the input uncertainties is represented using the non-intrusive polynomial chaos approach, where the deterministic coefficient functions are determined by discretizing the probability space with dimension adaptive sparse grids.

$$f_{PC}(p, s_d(\cdot, \zeta)) = \sum_{i=1}^{N_{PC}} \tilde{f}_i(p) \cdot \Phi_i(X_1, \dots, X_d)$$

3. The lower level problem is solved by a discretization approach based on locally refined sparse grids.

$$s_0 = \operatorname{argmin}_{s_d \in H} h(p, s_d)$$

4. The generalized, parallelized version of the one-shot algorithm is applied to solve the resulting discretized robust optimization problem.

$$\begin{aligned} \min_{y_i, p} \sum_{i=1}^N f(y_i, p, s_i) \omega_i \\ \text{s.t.} \quad c(y_i, p, s_i) = 0, \quad \forall i \in \{0, \dots, N\} \\ h(y_0, p, s_0) \geq 0, \end{aligned}$$

8 Numerical Results

In this section, numerical results will be presented investigating and comparing the influence of the robust measures introduced in section 4.

8.1 Definition of the deterministic aerodynamic shape optimization problem (2D Euler test case)

For this purpose, we consider the robust shape optimization of a RAE2822 profile in transonic Euler flow by the use of the unstructured flow solver TAU (cp. [69, 28]). In our example, the space is discretized by a 193×33 grid, see figure 1. For parametrization, the airfoil

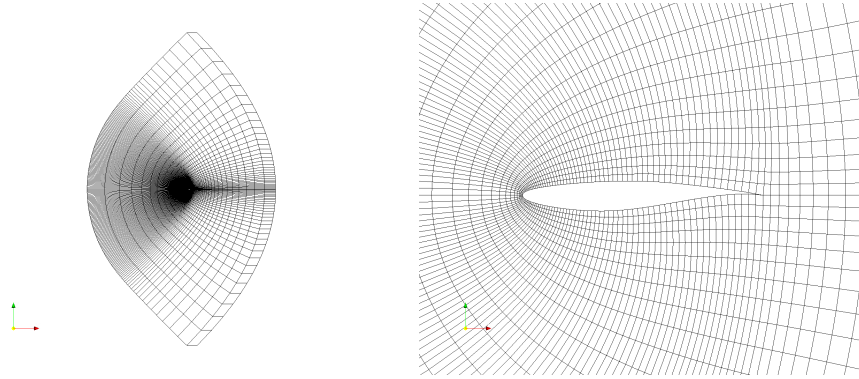


Fig. 1 C-type grid for the RAE2822 airfoil (Euler flow): the total geometrical plane (left) and zoom around the airfoil (right).

is decomposed into thickness and camber distribution. Then, only the camber of the airfoil is parametrized by 21 Hicks-Henne functions and the thickness is not changed during the optimization process.

The deterministic optimization problem is defined by

$$\min_{y,p} f(y,p) \quad (54)$$

$$\text{s.t. } c(y,p) = 0 \quad (55)$$

$$h(y,p) \geq 0 \quad (56)$$

with $p \in \mathbb{R}^{21}$, $y \in \mathbb{R}^{25476}$. The objective function f denotes the drag coefficient C_D , c is the steady state Euler equation with appropriate boundary conditions and the inequality constraint is defined by

$$h(y,p) = C_L(y,p) - C_L^0 \quad (57)$$

with $C_L^0 = 0.816$. The shape of the RAE2822 airfoil is to be optimized for transonic flight conditions, i.e.

$$M = 0.73, \quad \alpha = 2^\circ. \quad (58)$$

The initial values of the drag and lift coefficients are

$$C_D = 4.76 \cdot 10^{-3}, \quad C_L = 0.816.$$

A single-setpoint optimization using the one-shot method leads to the coefficients

$$C_D = 3.45 \cdot 10^{-3}, \quad C_L = 0.816,$$

which show a significant reduction of the drag coefficient.

8.2 Stochastic model of the geometrical uncertainties (2D Euler test case)

We consider now the deterministic shape optimization problem under geometrical uncertainties defined as follows. The perturbations of the shape are described by a transformed Gaussian random field $s : \Gamma \times \mathcal{O} \rightarrow \mathbb{R}$, where the Gaussian random field $\psi : \Gamma \times \mathcal{O} \rightarrow \mathbb{R}$ is given by

$$\mathbb{E}(\psi(x, \zeta)) = 0, \quad cov(x, y) = \sigma(x) \sigma(y) \exp\left(-\frac{\|x - y\|^2}{l^2}\right) \quad (59)$$

with $\sigma(x) = (0.8 - x_1)^{0.75}$ and $l = 0.005$. To ensure the boundedness, ψ is transformed to marginal sine-shaped distribution

$$s(x, \zeta) = c(x) \cdot \arccos(1 - 2\Phi(\psi(x, \zeta))) \quad (60)$$

with $c(x) = (0.8 - x_1)^{0.75} \cdot \sqrt{0.00002}$ controlling the limit of the perturbations. As mentioned before, no measurements are at hand to determine the stochastic model of the geometrical uncertainties. The assumptions made are discussed with engineers, so that the models reflect the main characteristics of uncertainties. Nevertheless, the description of the uncertainties need to be adapted to real-world data measuring the uncertainties occurring in the aerodynamical framework. But we want to point out here the fact that the methodology proposed in this paper does not rely on the special structure of the transformation and hence, the application to arbitrary stochastic models of the uncertainties is straightforward. The following figure shows three random realizations of the Gaussian random field ψ , which are then transformed to a sine-shaped distribution according to (60).

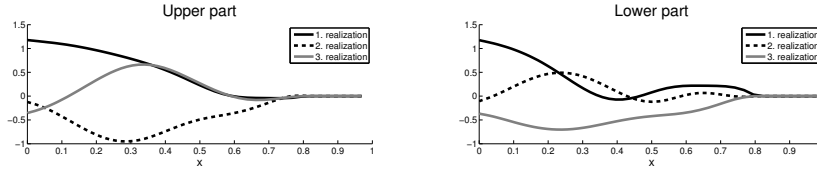


Fig. 2 Realizations of the Gaussian random field shown on the upper part of the surface (left) and lower part (right).

The resulting transformed realizations are depicted in Figure 3.

Further, the corresponding perturbed shapes are shown in Figure 4. Note that no perturbations arise in the back part of the airfoil ensuring the convergence of the flow solver, which is very sensitive to perturbations of the trailing edge.

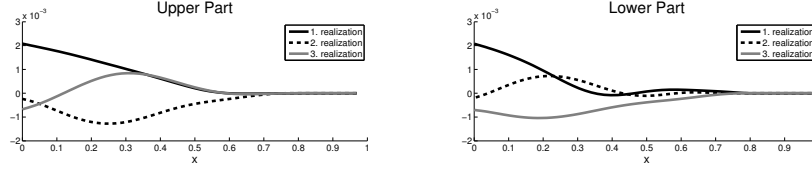


Fig. 3 Realizations of the transformed random field shown on the upper part of the surface (left) and lower part (right).

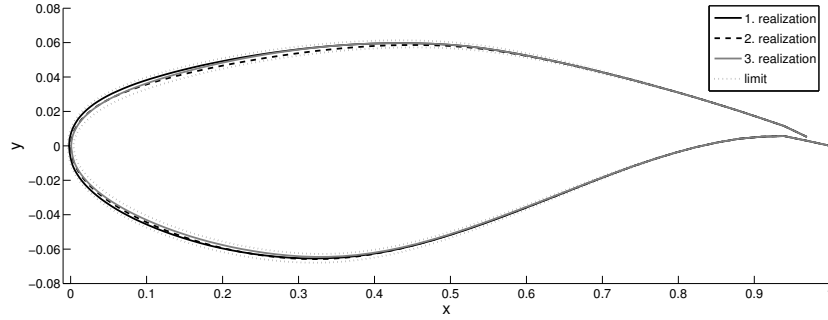


Fig. 4 Resulting perturbed shapes and bounds of the perturbations (dotted line in gray).

8.3 Approximation of the input random field using a goal-oriented Karhunen-Loève basis (2D Euler test case)

For the numerical treatment, the input Gaussian random field ψ is approximated in a finite number of random variables using the Karhunen-Loève expansion leading to

$$\psi_9(x, \zeta) = \sum_{i=1}^9 \sqrt{\lambda_i^{KL}} z_i^{KL}(x) X_i(\zeta), \quad (61)$$

where the distribution of the eigenvalues and the corresponding first 9 eigenvectors are depicted in Figure 5. The Karhunen-Loève expansion of order 9 (cf. (61)) involves eigenvectors with corresponding eigenvalues greater than 10^{-2} , which corresponds to 99.98% of the characteristics (in the discrete setting). The influence of the individual eigenvectors weighted by the eigenvalues is now investigated in order to choose the reduced Karhunen-Loève basis. The influence of the first 9 eigenvectors on the drag performance as well as the corresponding indicator are shown in Figure 6. The 6th – 9th weighted eigenvectors have no impact on the target functional, so that they can be rejected from the Karhunen-Loève basis and we obtain the following reduced basis

$$\psi_5(x, \zeta) = \sum_{i=1}^5 \sqrt{\lambda_i^{KL}} z_i^{KL}(x) X_i(\zeta). \quad (62)$$

A similar behavior can be observed investigating the lift performance with respect to Karhunen-Loève basis (cf. Figure 7). Again, the 1st – 5th eigenvector generate the reduced basis. An

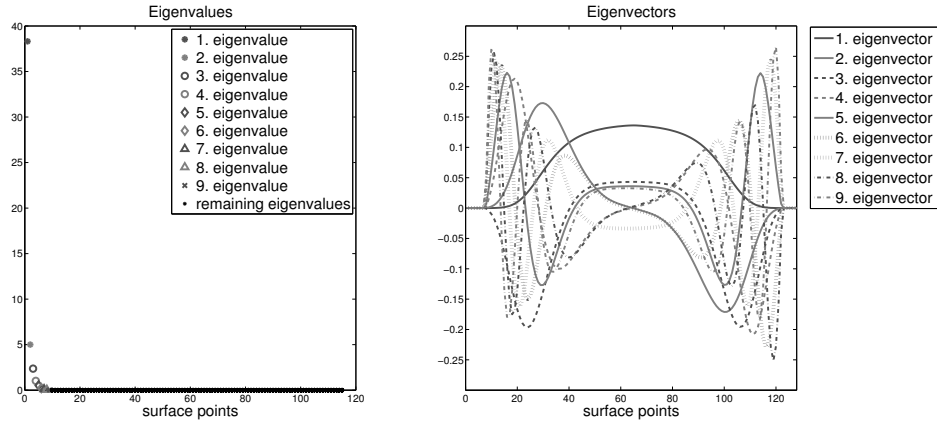


Fig. 5 Distribution of the eigenvalues (left) and corresponding first 9 eigenvectors (right).

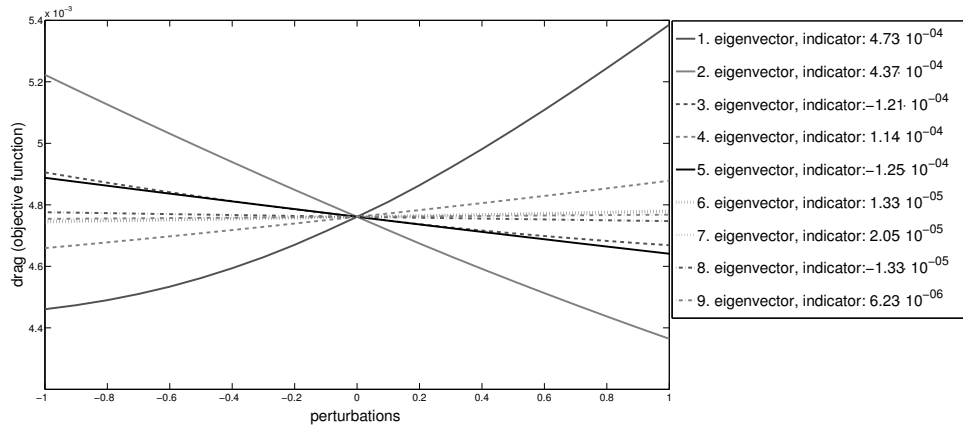


Fig. 6 Influence of the first 9 weighted eigenvectors on the drag performance and corresponding adaptivity indicator.

individual consideration of the influence on the drag as well as on the lift performance guarantees the approximation of both quantities, i.e. two reduced basis are obtained, one to quantify the influence on the drag and one to handle the robust constraint. In the given 2D test case, both reduced basis coincide and (63) can be used to approximate the quantities of interest with respect to the geometrical uncertainties.

For the purpose of demonstrating the approximation quality and efficiency of the proposed methodology as well as of comparing the introduced robustness measures, we will restrict the

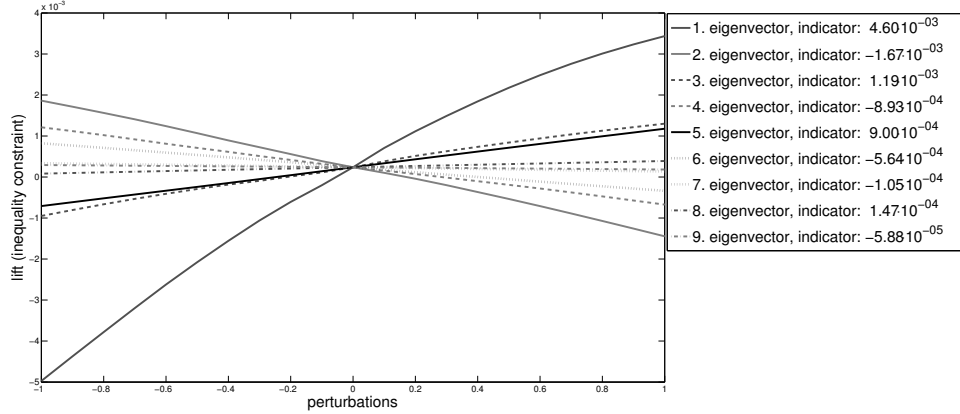


Fig. 7 Influence of the first 9 weighted eigenvectors on the lift constraint and corresponding adaptivity indicator.

discussion to the two dimensional case from now on, i.e. we assume that the input uncertainties can be approximated by

$$\psi_2(x, \zeta) = \sum_{i=1}^2 \sqrt{\lambda_i^{KL}} z_i^{KL}(x) X_i(\zeta). \quad (63)$$

This simplification allows us to compare the solution based on the introduced adaptivity strategies with a solution based on full tensor grids serving as a reference solution. Due to the complexity of the application of interest, this verification is impossible in the higher dimensional case.

8.4 Polynomial chaos approximation of the drag performance (2D Euler test case)

First of all, results studying the approximation quality of a polynomial chaos approximation based on dimension adaptive sparse grids in order to quantify the effects of geometrical uncertainties modeled by (63) on the drag performance will be presented. The polynomial chaos coefficients are determined by a dimension adaptive sparse grid using as adaptivity indicator the maximum error over all coefficient functions. The resulting grid compared to a full tensor grid, both based on Gauß- Hermite polynomials, which are the optimal choice considering normally distributed uncertainties (cf. (63) and (30), respectively), is depicted in Figure 8. The adaptive sparse grid consists of 41 grid points, where the full tensor grid based on a Gauß- Hermite quadrature of order 15 consists of 225 grid points, i.e. a reduction factor of 5 can be obtained. As no analytical solution is available in the application of interest, the solution based on the full tensor grid serves as reference solution. As mentioned before, the input uncertainties are approximated by normally distributed random variables resulting from the Karhunen-Loève expansion, so that the orthogonal polynomials in the polynomial chaos representation can be identified as Hermite polynomials. shown up to total order 3 in Figure 9.

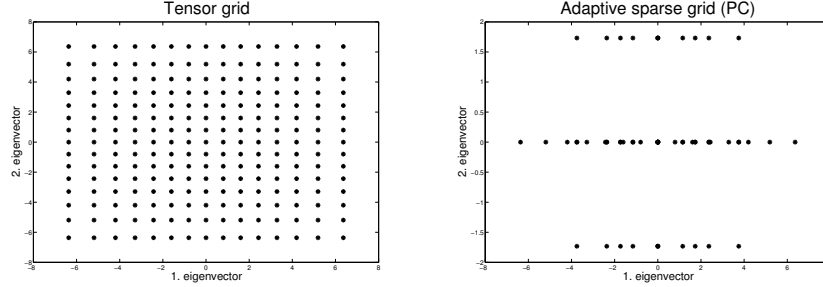


Fig. 8 Full tensor grid (left) and dimension adaptive sparse grid (right) used to determine the deterministic polynomial chaos coefficients.

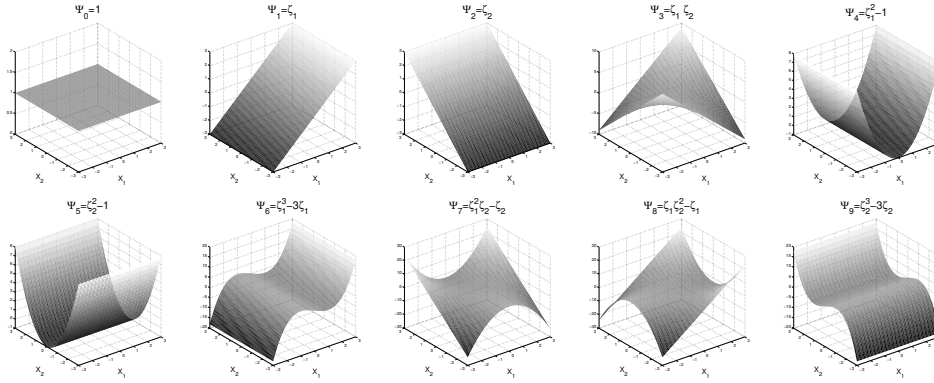


Fig. 9 2D Hermite polynomials up to total order 3.

The following figures compare the solution obtained by a polynomial chaos representation with respect to the truncation order with the reference solution, where the absolute error as well as the error weighted by the probability density function is chosen to indicate the approximation quality.

As Figure 13 indicates, an approximation of total order 3 leads to a fully satisfactory result, the maximum absolute error in the considered subdomain is less than $4 \cdot 10^{-4}$ and the weighted error less than $5 \cdot 10^{-6}$. Hence, it is sufficient to consider a truncation order of 3 in the optimization procedure.

8.5 Treatment of the lift constraint (2D Euler test case)

In the robust counterpart of the deterministic problem (54 - 55), we consider the following robust treatment of the constraint

$$h(y(s(X_1, X_2)), p, s(X_1, X_2)) \geq 0, X_{1,2} \in [-1, 1], \quad (64)$$

cf. (27). The arising lower level problem

$$s_0 = \underset{X_{1,2} \in [-1, 1]}{\operatorname{argmin}} h(y(s(X_1, X_2)), p, s(X_1, X_2)) \quad (65)$$

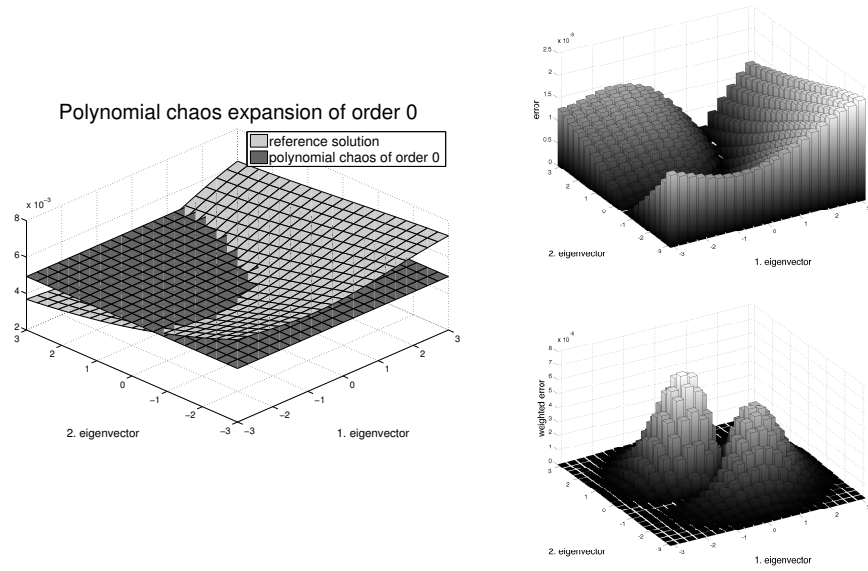


Fig. 10 Polynomial chaos approximation of total order 0 compared to reference solution (left), the absolute error (right above) and weighted error (right below).

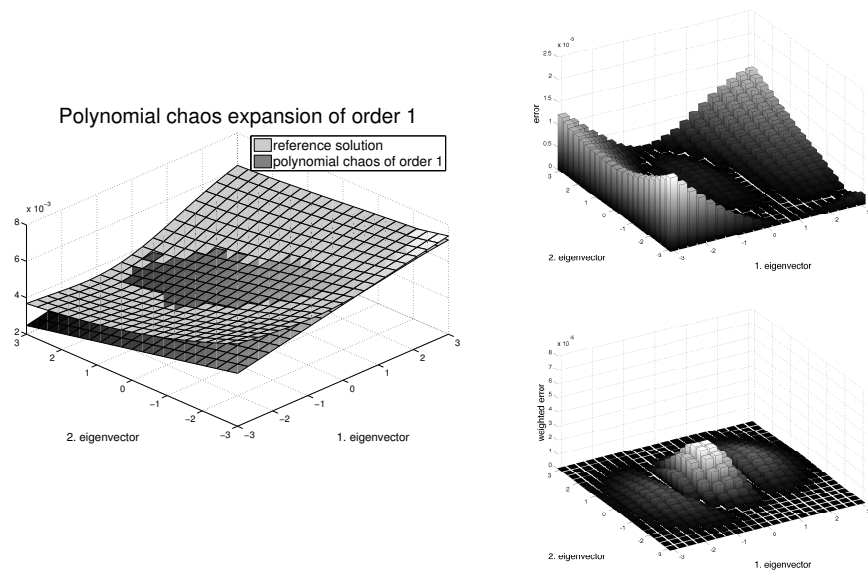


Fig. 11 Polynomial chaos approximation of total order 1 compared to reference solution (left), the absolute error (right above) and weighted error (right below).

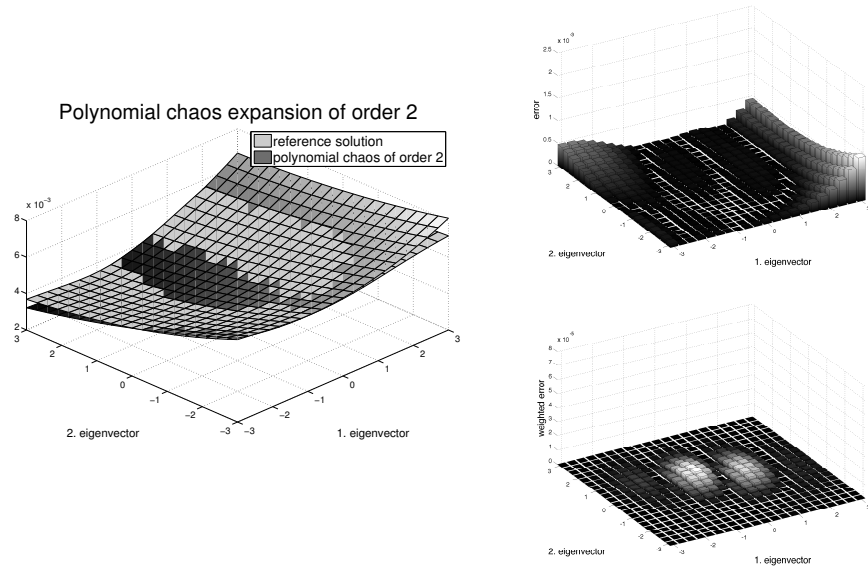


Fig. 12 Polynomial chaos approximation of total order 2 compared to reference solution (left), the absolute error (right above) and weighted error (right below).

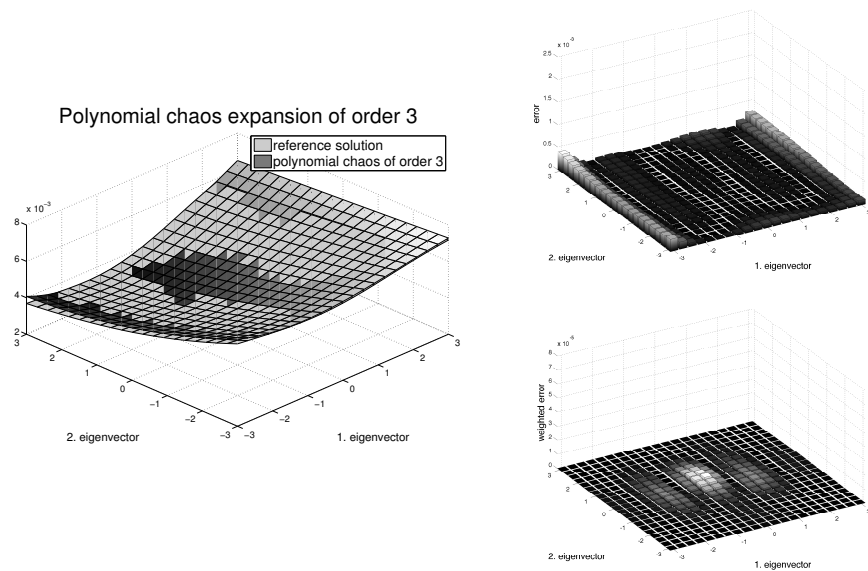


Fig. 13 Polynomial chaos approximation of total order 3 compared to reference solution (left), the absolute error (right above) and weighted error (right below).

is solved by a discretization approach based on locally refined sparse grids. In literature, a common approach to solve robust constraints of the form (27) is to assume that the solution of the lower level problem is always located at the boundary of the set H , in the given test case $[-1, 1]^2$. Although this is the case considering (64) due to the almost linear behavior of the lift constraint in the neighborhood of the nominal point (i.e. the unperturbed shape), we propose a discretization approach in order to handle arbitrary sets H without imposing the aforementioned, strict assumption. Figure 14 illustrates the lift performance in the domain $[-1, 1]^2$ as well as the corresponding locally refined sparse grid based on hierarchical linear ansatz functions.

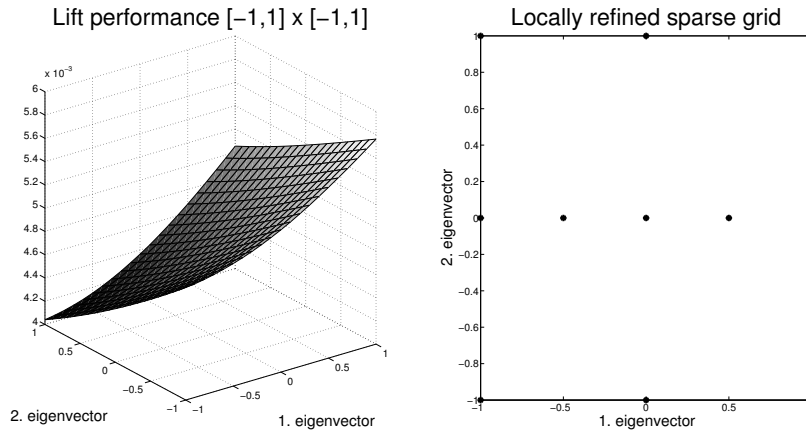


Fig. 14 Lift performance with respect to the two random input variables (left) and corresponding locally refined sparse grid (right).

Due to the almost linear behavior of the lift constraint, a coarse grid consisting of 11 grid points leads to an accurate surrogate model, which is then used to solve the lower level problem.

8.6 Verification of the proposed optimization method based on adaptive strategies (2D Euler test case)

In order to verify and demonstrate the efficiency of the proposed method, the following robust counterpart of the deterministic aerodynamic shape optimization problem (54-56) is considered

$$\min_{y(s(X_1, X_2)), p} \mathbb{E}(f(y(s(X_1, X_2)), p, s(X_1, X_2))) \quad (66)$$

$$\text{s.t.} \quad c(y(s(X_1, X_2)), p, s(X_1, X_2)) = 0, \forall X_1, X_2 \quad (67)$$

$$h(y(s(X_1, X_2)), p, s(X_1, X_2)) \geq 0, X_{1,2} \in [-1, 1] \quad , \quad (68)$$

where the mean value of the drag performance is chosen as robustness measure in the objective function. The solution of problem (66 - 68) is computed by the proposed method (cf. summary 7) as well as by an one-shot optimization using full tensor grids in order to quantify the influence of the input uncertainties. Both optimization strategies lead to comparable

drag performances of the optimized shapes (cf. Figure 15) and the optimized mean values are identical with respect to the precision of the flow solver, $\mathbb{E}_{adaptive}^{opt} = 4.152 \cdot 10^{-3}$ and $\mathbb{E}_{tensor}^{opt} = 4.135 \cdot 10^{-3}$. Further, we can observe that both solutions are feasible over the

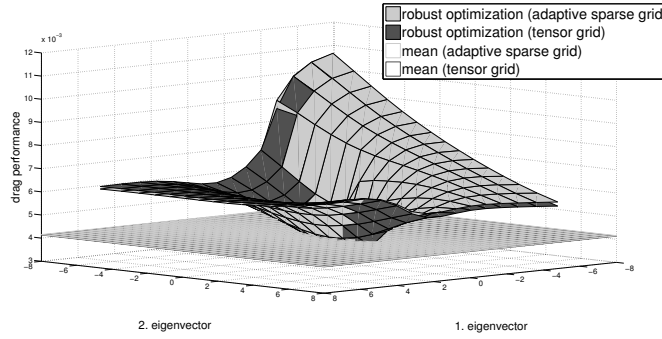


Fig. 15 Drag performances of the optimized shapes based on adaptive strategies (light gray) and full tensor grids (dark grey).

whole range of variations, as required (cf. Figure 16) and the resulting optimal shapes are completely identical (see Figure 17).

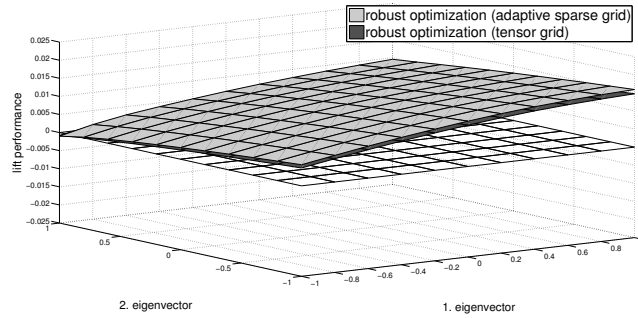


Fig. 16 Lift performances of the optimized shapes based on adaptive strategies (light gray) and full tensor grids (dark grey).

Summarizing, we can state that we could numerically prove the approximation quality and efficiency of the proposed method by comparing the solution to a full tensor grid optimization serving as reference solution.

The last part of this section is devoted to the study of the influence considering beside the mean value a combination of mean and variance as well as the expected excess as robustness measure in the objective function.

8.7 The influence of robustness measures on the optimal shape (2D Euler test case)

A difficult task in the context of robust optimization is to formulate the appropriate robust counterpart of the deterministic optimization problem. We will discuss in the following the

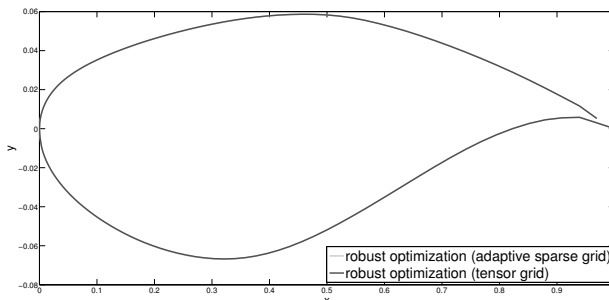


Fig. 17 Drag performances of the optimized shapes based on adaptive strategies (light gray) and full tensor grids (dark grey).

influence of robustness measures introduced in section 4 on the solution and demonstrate the applicability of the proposed method to the resulting optimization problems.

We start the discussion by again considering the optimization of the mean

$$\begin{aligned} & \min_{y(s(X_1, X_2)), p} \mathbb{E}(f(y(s(X_1, X_2)), p, s(X_1, X_2))) \\ \text{s.t.} \quad & c(y(s(X_1, X_2)), p, s(X_1, X_2)) = 0, \forall X_1, X_2 \\ & h(y(s(X_1, X_2)), p, s(X_1, X_2)) \geq 0, X_{1,2} \in [-1, 1] \quad . \end{aligned}$$

The characteristics of the robust solution will be now compared to the ones of the single-setpoint optimized shape. Figure 18 illustrates the drag performance of both solutions with respect to the input uncertainties. The single-setpoint optimization leads to a target value of

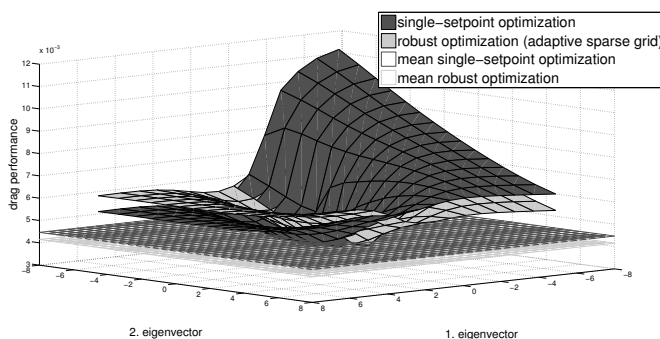


Fig. 18 Drag performances of the optimized shapes resulting from the robust optimization based on (66 - 68) (light gray) and single-setpoint optimization (dark gray).

$\mathbb{E}_{single\text{-setpoint}}^{opt} = 4.469 \cdot 10^{-3}$, which can be reduced by the robust solution to $\mathbb{E}_{robust\text{mean}}^{opt} = 4.152 \cdot 10^{-3}$. Taking a look at the lift performance (see Figure 19), we can observe that the robust solution is feasible over the whole range of variations, as required, whereas the single-setpoint solution is infeasible in most parts of the considered domain of perturbations. Note that only small changes of the shape (see Figure 20) lead to a better performance with respect

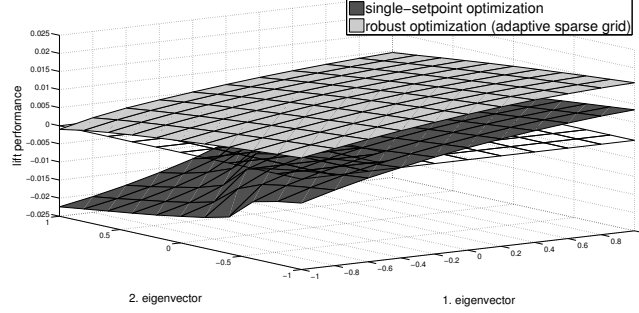


Fig. 19 Lift performances of the optimized shapes resulting from the robust optimization based on (66 - 68) (light gray) and single-setpoint optimization (dark gray).

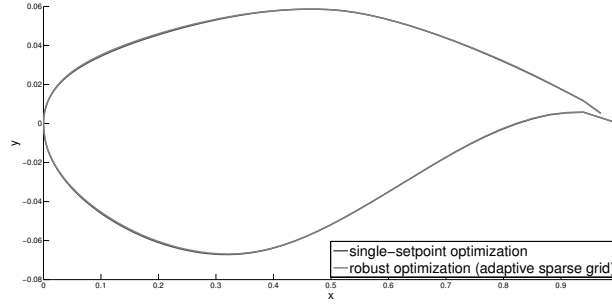


Fig. 20 Comparison of the optimized shapes resulting from the robust optimization based on (66 - 68) (light gray) and single-setpoint optimization (dark gray).

to the mean value as well as to feasibility in an enlarged domain.

Next, a combination of mean and variance as robustness measure will be studied, i.e. the following robust counterpart

$$\min_{y(s(X_1, X_2)), p} \mathbb{E}(f(y(s(X_1, X_2)), p, s(X_1, X_2))) + c\mathbb{V}(f(y(s(X_1, X_2)), p, s(X_1, X_2))) \quad (69)$$

$$\text{s.t.} \quad c(y(s(X_1, X_2)), p, s(X_1, X_2)) = 0, \forall X_1, X_2 \quad (70)$$

$$h(y(s(X_1, X_2)), p, s(X_1, X_2)) \geq 0, X_{1,2} \in [-1, 1] \quad (71)$$

is considered for a given parameter c indicating the risk aversion, that means a large coefficient c results in a more conservative design of the underlying optimization problem.

The numerical results presented below compare the robust solutions of problem (69 - 71) for three different values of the parameter c controlling the risk aversion of the designs, i.e. $c_1 = 10^3$, $c_2 = 10^4$ and $c_3 = 10^5$. First, we can observe that the lift constraint is not influenced by the different risk measures in the objective function. As Figure 23 indicates, the lift performance of the three optimized airfoils is almost the same and the required lift is reached over the whole range of variations. However, the drag performances of the optimized shapes

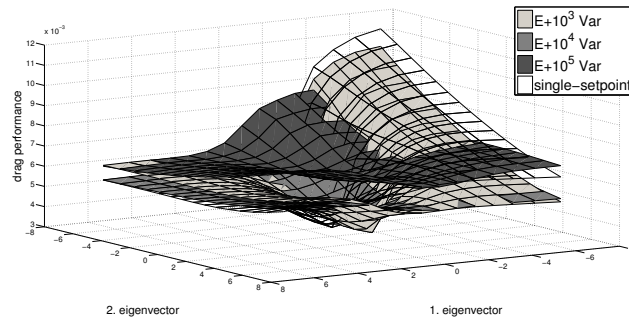


Fig. 21 Comparison of drag performance for different risk aversion values.

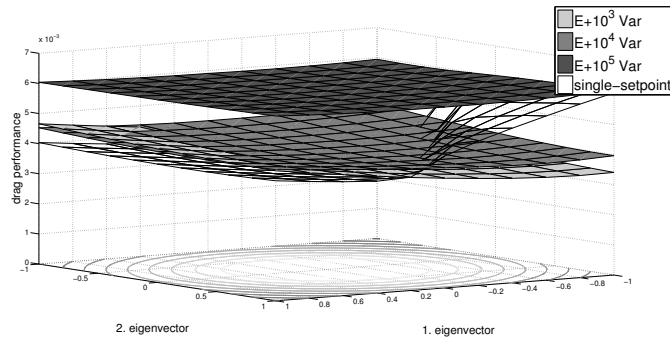


Fig. 22 Comparison of drag performance for different risk aversion values (zoom around the nominal point).

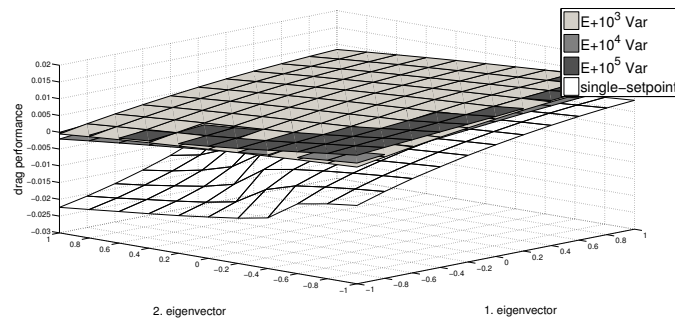


Fig. 23 Comparison of lift performance for different risk aversion values.

shown in Figure 21 and a zoom around the nominal point in Figure 22 clearly demonstrate the influence of the parameter c on the conservatism of the resulting airfoils. A high value of the risk aversion parameter c strongly penalizes a high value of the variance. Hence, the drag functions of the formulations with higher values of c get closer to the variance optimal

case, that means a variance equals zero resulting in a constant drag over the whole range of variations.

Further, we can state that the variance reduction leads to a higher drag than the optimization of the mean value. The tradeoff between mean value and variance minimization is illustrated in Table 1.

Measure of robustness	Statistics	
	\mathbb{E}	Var
\mathbb{E}	$4.15 \cdot 10^{-3}$	$3.57 \cdot 10^{-7}$
$\mathbb{E} + 10^3 \cdot \text{Var}$	$4.10 \cdot 10^{-3}$	$2.55 \cdot 10^{-7}$
$\mathbb{E} + 10^4 \cdot \text{Var}$	$4.33 \cdot 10^{-3}$	$8.91 \cdot 10^{-8}$
$\mathbb{E} + 10^5 \cdot \text{Var}$	$6.06 \cdot 10^{-3}$	$2.22 \cdot 10^{-8}$

Table 1 Comparison of the mean value and variance resulting from the different risk measures.

Taking a look at the results in Table 1, we can state that the mean value optimization and the mean-variance reduction with risk aversion parameter $c = 10^3$ lead to almost the same mean and variance of the drag. Thus, the risk aversion parameter $c = 10^3$ seems to be too small to effect the results. On the other hand, the other two formulations with $c = 10^4$ and $c = 10^5$ show a significant reduction of the variance and an amount in the mean value differing quite strongly from the mean value optimization. Comparing the resulting optimized shapes (cf. Figure 24), the same effect can be observed.

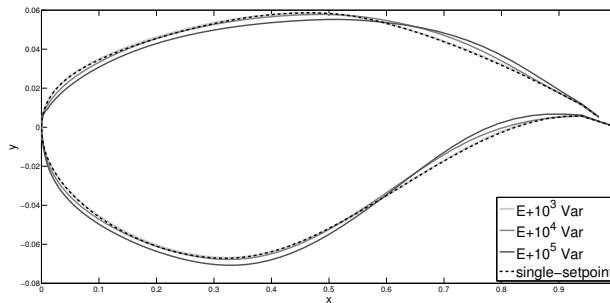


Fig. 24 Comparison of the resulting shapes optimized for different risk aversion values.

These investigations point out how important the proper choice of the risk aversion parameter c is. A too small value of the parameter c will not affect the results and a too large value may lead to overly conservative designs. In order to properly determine the value of the risk aversion parameter, additional knowledge on the magnitude of the variance and the mean as well as on the desired grade of robustness needs to be at hand.

The last part of this section concerns the robust optimization considering the expected excess as measure of robustness

$$\min_{y(s(X_1, X_2)), p} \mathbb{E}(\max\{f(y(s(X_1, X_2)), p, s(X_1, X_2)) - \eta, 0\}) \quad (72)$$

$$\text{s.t.} \quad c(y(s(X_1, X_2)), p, s(X_1, X_2)) = 0, \forall X_1, X_2 \quad (73)$$

$$h(y(s(X_1, X_2)), p, s(X_1, X_2)) \geq 0, X_{1,2} \in [-1, 1] \quad (74)$$

As mentioned above, the max-function in the objective (72) is replaced by a smooth approximation for practical convenience. The discretization of the probability space by the introduced adaptive polynomial chaos and by Monte Carlo techniques to approximate the expected excess based on the surrogate model leads to the following discretized optimization problem

$$\min_{y^i, p} \frac{1}{M} \sum_{i=1}^M \widehat{\max}\{f_{PC}^i(p) - \eta, 0\} \quad (75)$$

$$\text{s.t.} \quad c(y(s(X_1, X_2)), p, s(X_1, X_2)) = 0, \forall X_1, X_2 \quad (76)$$

$$h(y(s(X_1, X_2)), p, s(X_1, X_2)) \geq 0, X_{1,2} \in [-1, 1] \quad (77)$$

with $M = 10^8$. Again, the inequality constraint (77) is solved by a discretization approach based on locally refined sparse grids (cf. subsection 8). We investigate the influence of the robustness measure (72) and (75), respectively, for two values of the expected excess parameter η , i.e. $\eta = 4.15 \cdot 10^{-3}$, which corresponds to the optimized mean value, and $\eta = 4.4 \cdot 10^{-3}$. The drag performance of the two optimized shapes with respect to the expected excess parameter compared to the single-setpoint optimization are depicted in Figure 25. A zoom around

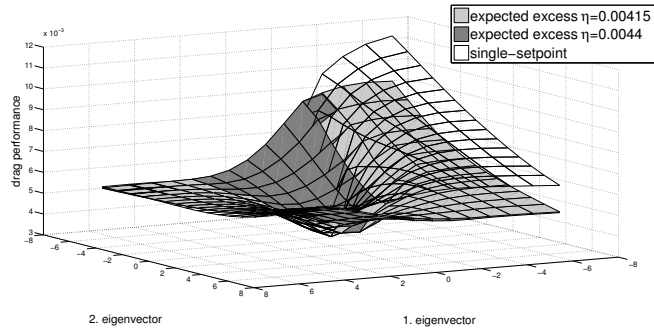


Fig. 25 Comparison of drag performance with respect to the expected excess parameter.

the nominal point (cf. Figure 26) shows the difference between the two solutions with respect to the expected excess parameter. Both solutions lead to a similar drag performance around the nominal resulting in a comparable objective value with $\eta = 4.15 \cdot 10^{-3}$. Considering the drag performance of the optimization with respect to $\eta = 4.4 \cdot 10^{-3}$, we can observe that the drag can be improved especially in the region near to $\eta = 4.4 \cdot 10^{-3}$ leading to a slightly better objective value than the solution with $\eta = 4.15 \cdot 10^{-3}$. The results are summarized in Table 2. Further, both solutions show feasibility over the whole range of variations, as required (cf.

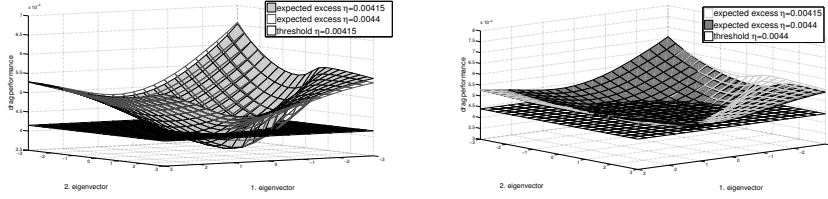


Fig. 26 Comparison of drag performance with respect to the expected excess parameter (zoom around the nominal point).

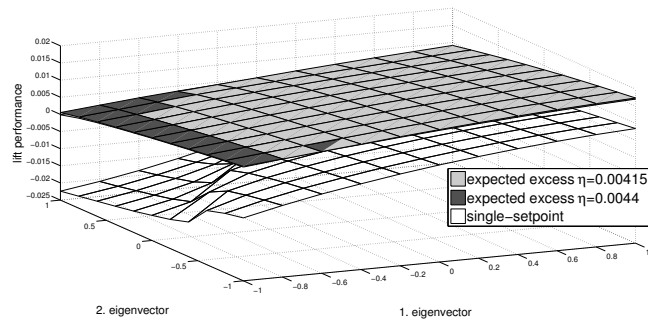


Fig. 27 Comparison of lift performance with respect to the expected excess parameter.

Figure 27).

Measure of robustness	Expected Excess	
	$\mathbb{E}_{EE} \eta=4.15 \cdot 10^{-3}$	$\mathbb{E}_{EE} \eta=4.4 \cdot 10^{-3}$
single-setpoint	$5.20 \cdot 10^{-4}$	$4.03 \cdot 10^{-4}$
$\mathbb{E}_{EE} \eta=4.15 \cdot 10^{-3}$	$1.33 \cdot 10^{-4}$	$6.41 \cdot 10^{-5}$
$\mathbb{E}_{EE} \eta=4.40 \cdot 10^{-3}$	$1.33 \cdot 10^{-4}$	$6.09 \cdot 10^{-5}$

Table 2 Comparison of the expected excess with respect to the expected excess parameter.

The resulting shapes are shown in Figure 28. As already observed, the robust optimization based on (72 - 74) with $\eta = 4.15 \cdot 10^{-3}$ and $\eta = 4.4 \cdot 10^{-3}$ leads to quite similar optimized shapes resulting in comparable objective values. A slight improvement can be stated in the case $\eta = 4.4 \cdot 10^{-3}$.

Finally, we will summarize the results of all robust optimizations in Table 3. Table 3 clearly reflects the influence of the discussed measure of robustness. If we take a look at the drag coefficients at the nominal point with respect to the introduced measure of robustness, we can observe an amount of the objective value with respect to the conservatism of the considered

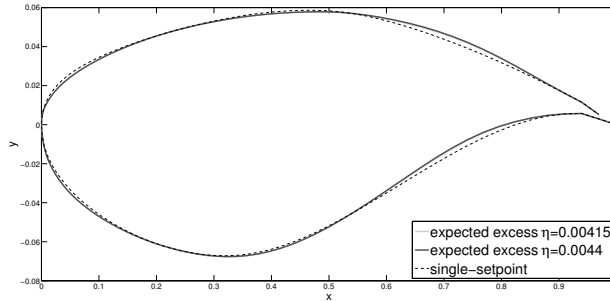


Fig. 28 Comparison of the optimized shapes resulting from the robust optimization based on (72 - 74) with $\eta = 4.15 \cdot 10^{-3}$ and $\eta = 4.4 \cdot 10^{-3}$, respectively and single-setpoint optimization.

Measure of robustness	Statistics				
	$f_{nominal}$	\mathbb{E}	Var	$\mathbb{E}_{EE \eta=4.15 \cdot 10^{-3}}$	$\mathbb{E}_{EE \eta=4.4 \cdot 10^{-3}}$
single-setpoint	$3.45 \cdot 10^{-3}$	$4.47 \cdot 10^{-3}$	$1.13 \cdot 10^{-6}$	$5.20 \cdot 10^{-4}$	$4.03 \cdot 10^{-4}$
\mathbb{E}	$3.75 \cdot 10^{-3}$	$4.15 \cdot 10^{-3}$	$3.57 \cdot 10^{-7}$	$1.94 \cdot 10^{-4}$	$1.19 \cdot 10^{-4}$
$\mathbb{E} + 10^3 \cdot Var$	$3.81 \cdot 10^{-3}$	$4.10 \cdot 10^{-3}$	$2.55 \cdot 10^{-7}$	$1.73 \cdot 10^{-4}$	$9.90 \cdot 10^{-5}$
$\mathbb{E} + 10^4 Var$	$4.04 \cdot 10^{-3}$	$4.33 \cdot 10^{-3}$	$8.91 \cdot 10^{-8}$	$2.18 \cdot 10^{-4}$	$9.13 \cdot 10^{-5}$
$\mathbb{E} + 10^5 \cdot Var$	$5.93 \cdot 10^{-3}$	$6.06 \cdot 10^{-3}$	$2.22 \cdot 10^{-8}$	$1.91 \cdot 10^{-3}$	$1.66 \cdot 10^{-3}$
$\mathbb{E}_{EE \eta=4.15 \cdot 10^{-3}}$	$3.77 \cdot 10^{-3}$	$4.13 \cdot 10^{-3}$	$1.26 \cdot 10^{-7}$	$1.33 \cdot 10^{-4}$	$6.41 \cdot 10^{-5}$
$\mathbb{E}_{EE \eta=4.40 \cdot 10^{-3}}$	$3.81 \cdot 10^{-3}$	$4.16 \cdot 10^{-3}$	$1.09 \cdot 10^{-7}$	$1.33 \cdot 10^{-4}$	$6.09 \cdot 10^{-5}$

Table 3 Comparison of the mean value and variance resulting from the different risk measures.

objective function, i.e. the tradeoff between the performance at the nominal point and the robustness of the solution. Considering the mean-variance optimization, the risk aversion parameter controls the robustness of the solution in terms of variance optimality, so that this parameter has to be carefully chosen in order to achieve the desired grade of robustness. The expected excess as measure of robustness reveals the same tendency in a weakened form. Further, we can state that the consideration of mean-risk measures in the formulation of the robust counterpart of the aerodynamic shape optimization problem leads to designs, which show a similar performance in the mean value compared to a sole minimization of the mean and, moreover, a reduction in the variance and expected excess. The proposed methodology allows to achieve this additional gain of robustness with the same computational costs as a sole minimization of the mean, so that the mean-risk models provide an attractive way for the formulation of the robust optimization problem.

Last, we will compare the shapes resulting from the single-setpoint optimization, mean value approach and from the mean-risk models.

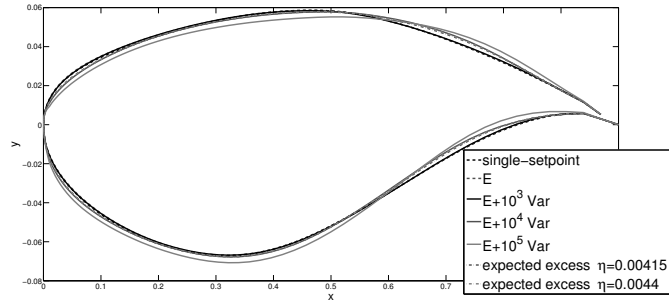


Fig. 29 Comparison of the resulting shapes optimized for different robustness measures.

As already stated, the variance reduction leads to the most conservative designs and therefore differ the most from the deterministic case (cf. Figure 29).

9 Conclusions

We proposed in this paper a methodology to efficiently handle a class of robust counterparts of the deterministic aerodynamic shape optimization problem including mean-risk models as measure of robustness and a robust treatment of additional constraints. The main ingredients of the methodology are a goal-oriented Karhunen-Loève expansion, a non-intrusive polynomial chaos model combined with adaptive sparse grid techniques and efficient optimization methods, in particular a generalized, parallelized one-shot approach. The discussed modifications and improvements as well as the proper use of adaptivity leads to an approach enabling the treatment of uncertainties in complex optimization problems. In the numerical results, we demonstrated and numerically verified the reliability and efficiency considering the robust optimization in a 2D test case under geometrical uncertainties. We further investigated the influence of different measure of robustness on the resulting optimized shapes. The study clearly showed the impact of the robustness measure on the conservatism of the resulting shapes, so that the proper choice of the robust formulation plays an important role in order to achieve the desired grade of robustness. Sophisticated mean-risk models allows to achieve the same drag performance in the mean as a sole minimization of the mean and, additionally, achieve an amount of robustness in terms of variance and expected excess reduction. This additional gain in robustness can be achieved with the same computational costs as a sole minimization of the mean using the proposed methodology. Hence, these models provide a very attractive way to formulate the robust counterpart of the aerodynamic shape optimization problem.

Acknowledgements This research has been partly supported by the German Federal Ministry of Economics and Labour (BMWA) within the collaborative effort MUNA under Contract No. 20A0604K.

References

- [1] S. AHMED AND A. SHAPIRO, *Solving chance-constrained stochastic programs via sampling and integer programming*, in TutORials in Operations Research, Z. L. Chen and S. Raghavan, eds.,

- INFORMS, 2008, pp. 261–269.
- [2] AIAA, *Guide for the verification and validation of computational fluid dynamics simulations*, American Institute of Aeronautics & Astronautics, 1998.
- [3] I. M. BABUSKA, F. NOBILE, AND R. TEMPONE, *A stochastic collocation method for elliptic partial differential equations with random input data*, SIAM Journal on Numerical Analysis, 45 (2007), p. 1005.
- [4] A. BEN-TAL, L. E. GHAOUI, AND A. NEMIROVSKI, *Robust Optimization*, Princeton Series in Applied Mathematics, Princeton University Press, October 2009.
- [5] D. BERTSIMAS AND M. SIM, *Tractable approximations to robust conic optimization problems*, Mathematical Programming, 107 (2006), pp. 5–36.
- [6] H.-G. BEYER AND B. SENDHOFF, *Robust optimization - a comprehensive survey*, Computer Methods in Applied Mechanics and Engineering, 196 (2007), pp. 3190–3218.
- [7] J. R. BIRGE AND F. LOUVEAUX, *Introduction to Stochastic Programming*, Springer, 1997.
- [8] H. BOCK, W. EGARTNER, W. KAPPIS, AND V. SCHULZ, *Practical shape optimization for turbine and compressor blades by the use of PRSQP methods*, Optimization and Engineering, 3 (2002), pp. 395–414.
- [9] H. BOCK, E. KOSTINA, A. SCHÄFER, J. SCHLÖDER, AND V. SCHULZ, *Multiple set point partially reduced SQP method for optimal control of PDE*, in Reactive Flows, Diffusion and Transport. From Experiments via Mathematical Modeling to Numerical Simulation and Optimization Final Report of SFB (Collaborative Research Center) 359, R. R. W. Jäger and J. Warnatz, eds., 2007.
- [10] H.-J. BUNGARTZ AND S. DIRNSTORFER, *Multivariate quadrature on adaptive sparse grids*, Computing, 71 (2003), pp. 89–114.
- [11] R. H. CAMERON AND W. T. MARTIN, *The orthogonal development of non-linear functionals in series of Fourier-Hermite functionals*, The Annals of Mathematics, 48 (1947), pp. 385–392.
- [12] L. EL GHAOUI, M. OKS, AND F. OUSTRY, *Worst-case value-at-risk and robust portfolio optimization: A conic programming approach*, Operations Research, 51 (2003), pp. 543–556.
- [13] M. ELDRED AND J. BURKARDT, *Comparison of non-intrusive polynomial chaos and stochastic collocation methods for uncertainty quantification*, in AIAA 47th Aerospace Sciences Meeting Including The New Horizons Forum and Aerospace Exposition, AIAA, 2009.
- [14] J. GARCKE, *A dimension adaptive sparse grid combination technique for machine learning*, in Proceedings of the 13th Biennial Computational Techniques and Applications Conference, CTAC-2006, W. Read, J. W. Larson, and A. J. Roberts, eds., vol. 48 of ANZIAM Journal, 2007, pp. 725 – 740.
- [15] J. GARCKE AND M. GRIEBEL, *Classification with sparse grids using simplicial basis functions*, Intelligent Data Analysis, 6 (2002), pp. 483–502.
- [16] J. GARCKE, M. GRIEBEL, AND M. TRESS, *Data mining with sparse grids*, Computing, 67 (2001), pp. 225–253.
- [17] N. GAUGER, *Das Adjungiertenverfahren in der aerodynamischen Formoptimierung*, PhD thesis, Technische Universität Braunschweig, 2003.
- [18] T. GERSTNER AND M. GRIEBEL, *Dimension-adaptive tensor-product quadrature*, Computing, 71 (2003), pp. 65–87.
- [19] R. G. GHANEM AND P. D. SPANOS, *Stochastic Finite Elements: A Spectral Approach*, Dover Publications, 2003.
- [20] I. GHERMAN, *Approximate Partially Reduced SQP Approaches for Aerodynamic Shape Optimization Problems*, PhD thesis, University of Trier, 2008.
- [21] M. B. GILES AND N. A. PIERCE, *Adjoint equations in CFD: Duality, boundary conditions and solution behaviour*, AIAA, 97 (1997).
- [22] ———, *An introduction to the adjoint approach to design*, Flow, Turbulence and Combustion, 65 (2000), pp. 393 – 415.
- [23] P. GLASSERMAN, *Monte Carlo Methods in Financial Engineering (Stochastic Modelling and Applied Probability)*, Springer, August 2003.

- [24] A. GRIEWANK, *Projected Hessians for preconditioning in one-step one-shot design optimization*, Nonconvex Optimization and its Application, 83 (2006), pp. 151–172.
- [25] C. R. GUMBERT, P. A. NEWMAN, AND G. J.-W. HOU, *Effect of random geometric uncertainty on the computational design of a 3D flexible wing*, in 20th AIAA Applied Aerodynamics Conference, 2002.
- [26] ———, *High-fidelity computational optimization for 3D flexible wings: Part II - effect of random geometric uncertainty on design*, Optimization and Engineering, 6 (2005), pp. 139 – 156.
- [27] J. HAMMERSLEY AND D. HANDSCOMB, *Monte Carlo Methods*, Methuen & Co, 1964.
- [28] R. HEINRICH, R. DWIGHT, M. WIDHALM, AND A. RAICHLER, *Algorithmic developments in TAU*, in MEGAFLOW - Numerical Flow Simulation for Aircraft Design, N. Kroll and J. Fassbender, eds., Springer, 2005, pp. 93–108.
- [29] R. HENRION, *Structural properties of linear probabilistic constraints*. Stochastic Programming E-Print Series, 2005.
- [30] R. M. HICKS AND P. A. HENNE, *Wing design by numerical optimization*, Journal of Aircraft, 15 (1978), p. 407412.
- [31] L. HUYSE, R. LEWIS, W. LI, AND S. PADULA, *Probabilistic approach to free-form airfoil shape optimization under uncertainty*, AIAA Journal, 40 (2002), pp. 1764–1772.
- [32] A. JAMESON, *Aerodynamic design via control theory*, Journal of Scientific Computing, 3 (1988), pp. 233–260.
- [33] ———, *Computational Aerodynamics for Aircraft Design*, Science, 245 (1989), pp. 361–371.
- [34] P. KALL AND S. WALLACE, *Stochastic Programming*, Wiley, Chichester, 1994.
- [35] K. KARHUNEN, *Zur Spektraltheorie stochastischer Prozesse*, Suomalaisen Tiedeakatemia toimituksia : Ser. A : 1, Mathematica, physica ; 34, 1946.
- [36] A. KLIMKE, *Uncertainty modeling using fuzzy arithmetic and sparse grids*, PhD thesis, Universität Stuttgart, Shaker Verlag, Aachen, 2006.
- [37] A. KLIMKE AND B. WOHLMUTH, *Algorithm 847: spinterp: Piecewise multilinear hierarchical sparse grid interpolation in MATLAB*, ACM Transactions on Mathematical Software, 31 (2005), pp. 561–579.
- [38] O. P. LE MAÎTRE AND O. M. KNIO, *Spectral Methods for Uncertainty Quantification: With Applications to Computational Fluid Dynamics (Scientific Computation)*, 1 ed., 2010.
- [39] C. LEMIEUX, *Monte Carlo and Quasi-Monte Carlo Sampling (Springer Series in Statistics)*, Springer, 1 ed., 2009.
- [40] W. LI, L. HUYSE, S. PADULA, AND L. R. CENTER., *Robust airfoil optimization to achieve consistent drag reduction over a mach range*, National Aeronautics and Space Administration, Langley Research Center, 2001.
- [41] W. LI AND S. L. PADULA, *Robust airfoil optimization in high resolution design space*, in ICASE NASA Langley Research Centre, 2003.
- [42] M. LOËVE, *Probability Theory 1*, Springer, 4 ed., 1977.
- [43] ———, *Probability Theory 2*, Springer, 4 ed., 1978.
- [44] G. LOEVEN, *Efficient uncertainty quantification in computational fluid dynamics*, PhD thesis, Technische Universiteit Delft, 2010.
- [45] ———, *Efficient uncertainty quantification in computational fluid dynamics*, PhD thesis, Technische Universiteit Delft, 2010.
- [46] G. LOEVEN AND H. BIJL, *Airfoil analysis with uncertain geometry using the probabilistic collocation method*, in 48th AIAA/ASME/ASCE/AHS/ASC Structures, Structural Dynamics, and Materials Conference, AIAA-2008-2070, 2008.
- [47] X. MA AND N. ZABARAS, *An adaptive hierarchical sparse grid collocation algorithm for the solution of stochastic differential equations*, Journal of Computational Physics, 228 (2009), pp. 3084–3113.
- [48] L. MATHELIN, M. HUSSAINI, AND T. ZANG, *Stochastic Approaches to Uncertainty Quantification in CFD Simulations*, Numerical Algorithms, 38-1 (2005), pp. 209–236.

-
- [49] H. MATTHIES, *Quantifying uncertainty: Modern computational representation of probability and applications*, in *Extreme Man-Made and Natural Hazards in Dynamics of Structures*, A. Ibrahim-begovic and I. Kozar, eds., vol. 21 of NATO Security through Science Series, Springer Netherlands, 2007, pp. 105–135.
- [50] M. MEYER AND H. MATTHIES, *Efficient model reduction in nonlinear dynamics using the Karhunen-Loève expansion and dual-weighted-residual methods*, *Computational Mechanics*, 31 (2003).
- [51] S. MISHRA, C. SCHWAB, AND J. UKYS, *Multi-level monte carlo finite volume methods for nonlinear systems of conservation laws in multi-dimensions*, *Journal of Computational Physics*, 231 (2012), pp. 3365 – 3388.
- [52] H. N. NAJM, *Uncertainty Quantification and Polynomial Chaos Techniques in Computational Fluid Dynamics*, *Annual Review of Fluid Mechanics*, 41 (2009), pp. 35–52.
- [53] H. NIEDERREITER, *Random number generation and Quasi-Monte Carlo methods*, Society for Industrial and Applied Mathematics, Philadelphia, USA, 1992.
- [54] W. L. OBERKAMPF, S. M. DELAND, B. M. RUTHERFORD, K. V. DIEGERT, AND K. F. ALVIN, *Error and uncertainty in modeling and simulation*, *Reliability Engineering & System Safety*, 75 (2002), pp. 333 – 357.
- [55] S. PADULA, C. GUMBERT, AND W. LI, *Aerospace applications of optimization under uncertainty*, *Optimization and Engineering*, 7 (2006), pp. 317–328.
- [56] O. PIRONNEAU, *On optimum design in fluid mechanics*, *Journal of Fluid Mechanics Digital Archive*, 64 (1974), pp. 97–110.
- [57] A. PRKOPA, *Stochastic Programming*, Kluwer Academic Publisher, 1995.
- [58] M. PUTKO, P. NEWMAN, A. TAYLOR III, AND L. GREEN, *Approach for uncertainty propagation and robust design in CFD using sensitivity derivatives*, in *AIAA 15-th Computational Fluid Dynamics Conference*, AIAA, 2001, pp. 2001–2528.
- [59] J. REUTHER, A. JAMESON, J. FARMER, L. MARTINELLI, AND D. SAUNDERS, *Aerodynamic shape optimization of complex aircraft configurations via an adjoint formulation*, Research Institute for Advanced Computer Science, NASA Ames Research Center, 1996.
- [60] A. RUSZCZYŃSKI AND A. SHAPIRO, *Stochastic Programming. Handbook in Operations Research and Management Science*, vol. 10, Elsevier, 2003.
- [61] ———, *Optimization of risk measures*, *Risk and Insurance*, EconWPA, 2004.
- [62] C. SCHILLINGS, *Optimal Aerodynamic Design under Uncertainties*, PhD thesis, Universität Trier, 2011.
- [63] C. SCHILLINGS, S. SCHMIDT, AND V. SCHULZ, *Efficient shape optimization for certain and uncertain aerodynamic design*, *Computers and Fluids*, 46 (2011), pp. 78 – 87. ;ce:title;10th ICFD Conference Series on Numerical Methods for Fluid Dynamics (ICFD 2010);/ce:title;.
- [64] S. SCHMIDT, C. ILIC, N. GAUGER, AND V. SCHULZ, *Shape gradients and their smoothness for practical aerodynamic design optimization*, Tech. Rep. SPP1253-10-03, DFG-SPP 1253, 2008. submitted (OPTE).
- [65] S. SCHMIDT AND V. SCHULZ, *Impulse response approximations of discrete shape Hessians with application in CFD*, *SIAM Journal on Control and Optimization*, 48 (2009), pp. 2562–2580.
- [66] V. SCHULZ AND I. GHERMAN, *One-shot methods for aerodynamic shape optimization*, in *MEGADESIGN and MegaOpt - Aerodynamic Simulation and Optimization in Aircraft Design*, N. Kroll, D. Schwamborn, K. Becker, H. Rieger, and F. Thiele, eds., Notes on Numerical Fluid Mechanics and Multidisciplinary Design, Springer, 2008.
- [67] V. SCHULZ AND C. SCHILLINGS, *On the nature and treatment of uncertainties in aerodynamic design*, *AIAA Journal*, 47 (2009), pp. 646 – 654.
- [68] C. SCHWAB AND R. A. TODOR, *Karhunen-loève approximation of random fields by generalized fast multipole methods*, *J. Comput. Phys.*, 217 (2006), pp. 100–122.
- [69] D. SCHWAMBORN, T. GERHOLD, AND R. HEINRICH, *The DLR TAU-code: Recent applications in research and industry*, in *European Conference on Computational Fluid Dynamics*, ECCOMAS CFD, 2006.

-
- [70] S. A. SMOLYAK, *Quadrature and interpolation formulas for tensor products of certain classes of functions*, Soviet Mathematics Doklady, 4 (1963), pp. 240–243.
 - [71] A. L. SOYSTER, *Convex programming with set-inclusive constraints and applications to inexact linear programming*, Operations Research, 21 (1973), pp. 1154–1157.
 - [72] S. TA'ASAN, G. KURUVILA, AND M. SALAS, *Aerodynamic design and optimization in one shot*, in 30th Aerospace Sciences Meeting, Reno, NV, AIAA Paper 92-0025, 1992.
 - [73] X. WAN AND G. E. KARNIADAKIS, *Multi-element generalized polynomial chaos for arbitrary probability measures*, SIAM Journal of Scientific Computing, 28 (2006), pp. 901–928.
 - [74] G. W. WASILKOWSKI AND H. WOZNIAKOWSKI, *Explicit cost bounds of algorithms for multivariate tensor product problems*, Journal of Complexity, 11 (1994), pp. 1–56.
 - [75] N. WIENER, *The homogeneous chaos*, American Journal of Mathematics, 60 (1938), pp. 897–936.
 - [76] D. XIU AND G. E. KARNIADAKIS, *The wiener–askey polynomial chaos for stochastic differential equations*, SIAM J. Sci. Comput., 24 (2002), pp. 619–644.
 - [77] D. W. ZINGG AND S. ELIAS, *On aerodynamic optimization under a range of operating conditions*, in 44th AIAA Aerospace Sciences Meeting, Reno, 2006.